https://doi.org/10.5194/egusphere-2026-2543
Preprint. Discussion started: 22 June 2026

The 2022 Rainfall-Triggered Landslide-Tsunami Disaster in Pilar, Abuyog, Leyte, Philippines and its implications for coastal hazard assessment

Likha G. Minimo[1,2], Janneli Lea A. Soria[3], Richard L. Ybañez[1,2], Audrei Anne B. Ybañez[1], Angelu B. Bermas[1], Kayla Milcah M. Marasigan[1], Adrian Gelo F. Tianchon[1], Jannine T. Vasquez[1], Victor M. Romero II[4], Allan Fitzgerald N. Amistoso[4], Christer Kim O. Gerona[4†], Genaro A. Cuaresma[5], and Alfredo Mahar Francisco A. Lagmay*[1,6]

[1]UP Resilience Institute and NOAH Center, University of the Philippines, Diliman, Quezon City, 1101, Philippines
[2]Science and Society Program, Science and Society Program, College of Science, University of the Philippines, Diliman, Quezon City, 1101, Philippines
[3]Mindanao State University at Naawan, Naawan, Misamis Oriental, 9023, Philippine (current affiliation)
[4]Regional Environmental Information System, University of the Philippines, Tacloban College, Tacloban City, 6500, Philippines
[5]Institute of Mathematical Sciences, College of Arts and Sciences, University of the Philippines, Los Baños, 4031, Philippines
[6]National Institute of Geological Sciences, College of Science, University of the Philippines, Diliman, Quezon City, 1101, Philippines
† deceased

Correspondence to: Likha G. Minimo (lgminimo@up.edu.ph)

Abstract. On 12 April 2022, a rainfall-triggered landslide in Barangay Pilar, Abuyog, Leyte, Philippines generated destructive tsunamis upon reaching the coast, resulting in one of the deadliest landslide disasters in the country's history. The event occurred during prolonged and intense rainfall associated with the interaction of a low pressure area, Severe Tropical Storm Megi (Agaton), and Typhoon Malakas (Basyang). The cascading rainfall–induced landslide–tsunami hazards caused 54 fatalities, injured 49 individuals, and left 33 persons missing and presumed dead, with tsunami inundation responsible for a substantial proportion of the losses. We reconstructed the event chronology and failure mechanisms using an integrated dataset comprising satellite imagery, unmanned aerial vehicle (UAV) surveys, field mapping, sedimentological analyses, and three-dimensional terrain modelling, eyewitness accounts, social media videos, and incident reports. Results indicate that two landslides with a total volume of around 5.5 x 10^5 m^3 were mobilized as debris flows. The landslides were composed of volcanic materials that originated from a fault-controlled ridge south of Pilar that reached the coast of Leyte Gulf. The initial and larger debris flow generated tsunami waves with runup heights of about 12 m above sea level, devastating residential areas along the coast and overwhelming people fleeing the landslide. Analysis of landslide–tsunami coupling indicates that wave generation was governed primarily by high-momentum impact conditions, with debris flow velocities of up to 25 m/s and short source-to-shore distances limiting energy dissipation prior to coastal entry. These conditions produced strongly supercritical

https://doi.org/10.5194/egusphere-2026-2543
Preprint. Discussion started: 22 June 2026

flow and demonstrate that relatively moderate-volume landslides can generate significant near-field tsunamis when velocity and proximity are favorable. This study is the first well-documented subaerial landslide-generated tsunami in the Philippines and provides a data-rich example of a rainfall-induced landslide–tsunami cascade in a tropical island setting. The Pilar disaster highlights the extreme hazard posed by rainfall-triggered landslides in steep coastal volcanic terrains and underscores the need to explicitly incorporate landslide–tsunami cascade scenarios into hazard assessment, early warning systems, and land-use planning in similar coastal regions.

1 Introduction

Landslide-generated tsunamis represent one of the most destructive yet least anticipated tsunami sources worldwide, particularly in steep coastal environments. While earthquake-generated tsunamis account for most documented events, landslides contribute disproportionately to tsunami-related fatalities because of their localized amplification, short warning times, and extreme runup heights (Harbitz et al., 2014; Løvholt et al., 2015; Reid and Mooney, 2023). Despite this, subaerial landslide tsunamis remain poorly documented in tropical island settings, where intense rainfall, volcanic terrains, and concentrated coastal settlements combine to create particularly high-risk conditions.

On 12 April 2022, a catastrophic rainfall-triggered coastal landslide in Barangay Pilar, Abuyog, Leyte, Philippines generated destructive tsunamis upon reaching the coast. The cascading hazard occurred following prolonged rainfall associated with the interaction of a low pressure area, Severe Tropical Storm Megi (Agaton), and Typhoon Malakas (Basyang). The event claimed 54 lives, injured 49 individuals, and left 33 missing and presumed dead in Barangay Pilar (Municipal Disaster Risk Reduction and Management Office-Abuyog, 2022; Leyte Provincial Disaster Risk Reduction and Management Office, 2022), marking it as one of the deadliest rainfall-induced landslide disasters in the country's history.

This study documents the first confirmed subaerial landslide-generated tsunami in the Philippines. We (1) reconstruct the chronology and mechanics of the Pilar landslide tsunami using field, UAV and satellite data, integrated with interviews, reports and video footage from responders and survivors; (2) characterize the landslide and tsunami runup in a semi-enclosed basin; and (3) discuss implications for landslide-tsunami hazard assessment and disaster risk reduction in volcanic island arcs.

2 Background: Landslide-Generated Tsunamis

Landslides are recognized as the second most frequent cause of tsunamis globally after earthquakes (Harbitz et al., 2014; Løvholt et al., 2020; Tappin, 2010). Landslide-generated tsunamis are commonly characterized by short wavelengths, strong spatial variability, and locally extreme runup heights, particularly in near-field settings (Okal and Synolakis, 2004; Løvholt et al., 2015; Heller and Ruffini, 2023).

https://doi.org/10.5194/egusphere-2026-2543
Preprint. Discussion started: 22 June 2026

Subaerial landslides entering water bodies such as seas, lakes, fjords, or reservoirs can generate impulsive waves capable of devastating coastal communities. Notable examples include the 1792 Mt. Mayuyama Debris Avalanche in Japan, the 1958 Lituya Bay landslide in Alaska, the 1963 Vajont landslide in Italy, the 2002 Sciara del Fuoco submarine-subaerial sequence of landslides at Stromboli, and the 2018 Anak Krakatau volcanic flank collapse in Indonesia (e.g., Katayama, 1974; Tan and Chen, 2017; Grilli et al., 2019; Casalbore et al., 2020; Heidarzadeh et al., 2020). While many well-studied cases occurred in confined basins or volcanic settings (Heller and Ruffini, 2023; Dohmen et al., 2025), rainfall-triggered landslide tsunamis are less documented (i.e., Aránguiz et al., 2023; Duc et al., 2020). The "Landslide Triggered Tsunamis" marked in the map by Dohmen et al. (2025) in the Philippines are described as historical and probable volcanic tsunamis in Taal Caldera, Babuyan Archipelago, or was "confused with storm surges" according to Paris et al. (2014). This documentation of the Pilar event contributes a rare, data-rich case study of a rainfall-induced, subaerial landslide tsunami in an island-arc setting. As the first well-documented event of its kind in the Philippines, it highlights the urgent need to improve hazard assessments in inhabited coastlines characterized by steep volcanic terrain.

3 Study Area and Geological Setting

Barangay Pilar is a coastal village within the municipality of Abuyog, Leyte, Philippines, fronting the Leyte Gulf (Fig. 1). The area is characterized by short, steep watersheds draining directly from mountainous terrain to the coast. Leyte Island lies within the Philippine Mobile Belt (PMB; Fig. 1a), a tectonically active zone resulting from the interaction of the Eurasian and Philippine Sea plates (Gervasio, 1971; Lagmay et al., 2009).

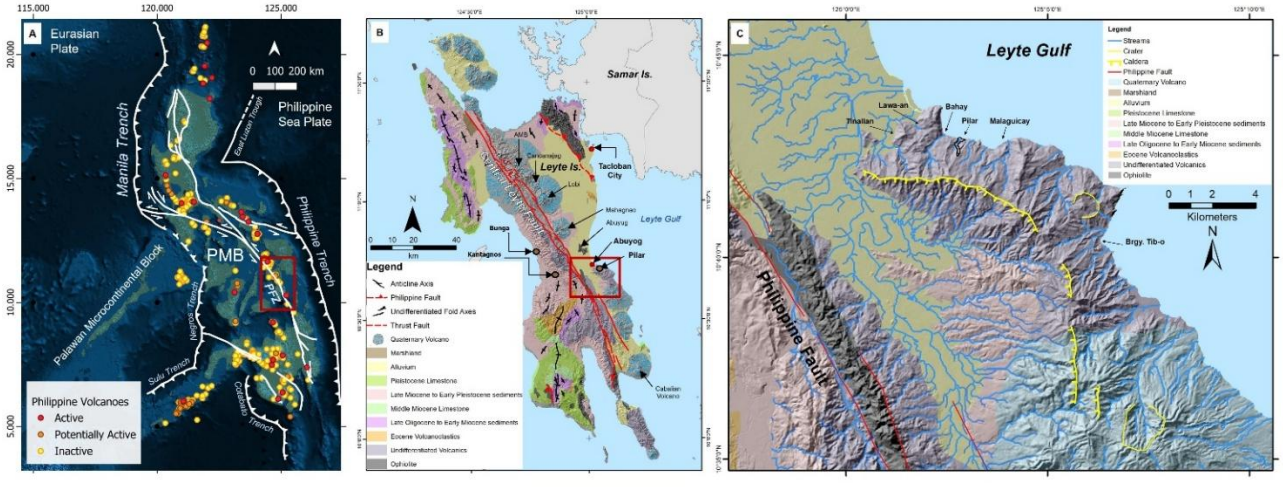

Figure 1: Location map of Barangay Pilar, Abuyog, Leyte, Philippines. A) Regional geologic and tectonic setting of Leyte (Tectonic structures and volcano locations modified from the Philippine Institute of Volcanology and Seismology, 2008a&b). B-C) Geologic map of Leyte island and Pilar area (modified from Sajona et. al., 1997). Basemap data sources: Elevation data from Shuttle Radar Topography Mission from the United States Geological Survey (USGS, 2004) and Interferometric Synthetic Aperture Radar Digital Terrain Model (IfSAR DTM) from National Mapping and Resource Information Authority (NAMRIA, 2013); bathymetric data from General Bathymetric Chart of the Oceans (GEBCO, 2009); and administrative boundaries modified from the Database of Global Administrative Areas (GADM, 2013).

https://doi.org/10.5194/egusphere-2026-2543
Preprint. Discussion started: 22 June 2026

The geology of central Leyte (Fig. 1b; modified from Sajona et al., 1997) is dominated by volcanic and volcaniclastic rocks ranging in age from Eocene to Holocene, including andesite, basalt, dacite, and pyroclastic deposits (Mines and Geosciences Bureau, 2010). The study area is underlain by the Pangasugan Formation, composed of poorly sorted conglomerates and volcaniclastics intruded by andesitic dikes (MGB, 2010; MGB-Region VIII, 2022). These lithologies are highly susceptible to weathering and slope failure under prolonged saturation.

The Central Leyte segment of the Philippine Fault Zone (PFZ in Fig. 1a; Allen, 1962; Philippine Institute of Volcanology, 2008) passes approximately 9 km west of Barangay Pilar (Fig.1c) and has produced prominent fault-related geomorphic features across the island (Tsutsumi and Perez, 2013). Fault-controlled fracturing and long-term geomorphic degradation likely contributed to slope instability in the landslide source area.

4 Data and Methods

This study integrates multiple datasets, including satellite imagery, UAV surveys, lithologic mapping, sediment characterization, eyewitness interviews, official incident reports, and social media videos documenting the event. These datasets were combined to reconstruct event chronology, characterize landslide dynamics, and assess tsunami generation and impact. Information on the weather conditions and hazard warnings in the region from March to April 2022 were collated along with online news articles, social media posts of residents, responders, and agencies like the Bureau of Fire (BFP) Region VIII, Philippine Atmospheric, Geophysical and Astronomical Services Administration (PAGASA), the Japan Aerospace Exploration Agency (JAXA), the Mines and Geosciences Bureau (MGB), Philippine Institute of Volcanology and Seismology (PHIVOLCS) and the UP Nationwide Operational Assessment of Hazards (UP NOAH). Hazards and their impacts were initially mapped from the incident reports of national, provincial, and local Disaster Risk Reduction and Management (DRRM) Councils and Offices and satellite data analysis of the Department of Science and Technology-Advanced Science and Technology Institute (DOST-ASTI), and the Philippine Space Agency (PhilSA). Whenever geographic locations are provided, the reported hazard incidents were plotted on a map (Supplementary file 1). Given the heterogeneous nature of these datasets, uncertainties arise from differences in spatial resolution, temporal coverage, and reporting accuracy, particularly for crowdsourced and social media-derived information. These uncertainties were minimized through cross-validation across independent data sources wherever possible.

Geological fieldwork, including site mapping, sample collection, and validation of remotely sensed observations, eye-witness interviews, and video footage gathering were conducted in July 2022 in Barangays Pilar, Bahay, and Malaguicay (Fig.1c). The local government only permitted entry into the landslide area three months after the event due to accessibility and safety issues. A total of 20 key informants (e.g., video owners, survivors, responders, local government officials) were interviewed in their local language (Tagalog, Cebuano, and Waray). With the informed consent of respondents, interviews were audio-recorded, transcribed, translated into English, and coded into themes and topics (Thomas, 2006). These qualitative data were used to

https://doi.org/10.5194/egusphere-2026-2543
Preprint. Discussion started: 22 June 2026

constrain event timing, sequence, and observed flow behavior. Whenever available, respondents also provided video footage of the landslide and/or tsunami. Details from official situational reports were integrated with informant narratives to reconstruct the timeline of events leading to the April 12, 2022, landslide and tsunami. Videos by first responders and vloggers were analysed for initial landslide extent, flow heights, directions and velocities, and tsunami wave periods. Video-derived measurements were obtained by tracking identifiable reference points (e.g., buildings, trees) across successive frames. Uncertainty in video-derived measurements arises from perspective distortion, camera motion, and scaling based on reference objects. These were reduced by selecting videos with stable viewpoints and clearly identifiable fixed features.

Field observations focused on landslide scarps, transport pathways, and landslide and tsunami wave characteristics. A key step was establishing the spatial extent of tsunami impact from that of the landslide deposits based on observed damage patterns. Houses that sustained partial structural damage, partial burial, and soil staining on walls were interpreted to mark the limit of debris flow inundation. From features like these we estimated velocities using runup heights (Eq.1):

$$v = \sqrt{2gh}\,, \tag{1}$$

where v is the flow velocity, g is the acceleration due to gravity, and h is the runup height. This approach assumes conversion of potential energy at maximum run-up into kinetic energy and provides a first-order estimate of flow velocity. Where applicable, we also used superelevation to estimate debris flow velocity (Eq.2):

$$v = \sqrt{gR\frac{\Delta h}{b}} \tag{2}$$

where v is the flow velocity, g is the acceleration due to gravity, R is the radius of curvature, Δh is the superelevation, and b is the channel width. Superelevation-based estimates were applied in channel bends where lateral flow deflection was evident. This assumption neglects energy losses due to turbulence, internal deformation, and friction, and therefore likely yields conservative (lower-bound) velocity estimates. Uncertainty in runup measurements (typically ±0.2–0.5 m) propagates into velocity estimates and is estimated to result in uncertainties on the order of ±10–20%.

Houses reduced to rubble, where only the floor remained intact, and no soil smudging was observed, were attributed to wave impact from the subsequent tsunami. Rafted debris lines and denuded cliffside were used to estimate the high-water mark and the extent of tsunami inundation (Fritz et al., 2007). The runup heights and inundation distances were estimated using a surveying measuring tape, GPS, and a laser rangefinder, following standard post-tsunami survey protocols (Fritz et al. 2007; Synolakis et al., 2005; United Nations Educational, Scientific and Cultural Organization, 2014). All measurements were referenced to mean sea level where possible.

Surface sediments from landslide deposits and potential tsunami deposits were acquired in Pilar. With the complexity of sedimentation processes in cascading landslide tsunami events, we rely on field observations to constrain the relative influence of each surface process on the corresponding deposit. Sediments found within the limit of the debris flow impact were classified as the debris flow deposit. On the other hand, the sediments beyond the debris flow impact limit and within the tsunami impact

https://doi.org/10.5194/egusphere-2026-2543
Preprint. Discussion started: 22 June 2026

zone are potential tsunami deposits. One main objective of this study is to constrain debris flow mechanics, as it is foundational to tsunami generation. As such, in this study, we will only focus on the sedimentology of the debris flow. Sedimentological analysis of tsunami deposits is reserved for future work involving numerical modelling of wave processes.

The Pilar debris flow deposits were mostly unconsolidated and exhibited a wide grain-size range, from coarse gravel to a substantial (>10%) mud fraction. Sediment grain-size distribution was determined using the standard wet-sieving method following Lewis and McConchie (2012), without pre-treatment. Sediments were washed through a stacked sieve column under running water. Material retained on each sieve was collected in evaporating dishes, dried at 60 °C for ≥24 h in a drying oven, and weighed using an OHAUS Pioneer PA213 analytical balance. The difference between the initial subsample mass and the cumulative mass of the retained fractions represents the finest particle fraction (<63 μm), which was allowed to pass through the sieve stack during washing. This procedure provides grain-size distribution across gravel to fine silt fractions.

Grain-size data were subsequently processed using GRADISTAT version 8.0 (Blott and Pye, 2001). The sediment fraction within each size class (e.g., clay, very coarse silt, medium sand), together with the logarithmic grain-size parameters, including mean, median, mode, sorting, and skewness (Folk and Ward,1957), were calculated for each sample and used to classify the different debris flow units. These parameters were used to distinguish between debris-flow phases and depositional environments.

Post-landslide digital elevation models were compared with a pre-landslide digital elevation model to estimate landslide volumes and erosion depths. High-resolution UAV imagery was acquired using DJI Mavic 2 Pro, Mavic Air, and Mavic 3 platforms. Orthophotos and digital surface models were generated using Pix4D software and used to map landslide extents and surface deformation (Ybañez et al., 2021). Pre- and post-event digital elevation models derived from a 2011 IfSAR (DTM; NAMRIA, 2013) and the July 2022 UAV survey were used to estimate landslide volumes and erosion depths. Elevation differencing was performed to quantify material removal and deposition (Supplementary File 2).

Using Leapfrog Geo, we constructed geological models of the landslide area from the 5-meter resolution 3D Digital Surface Models (DSM) from NAMRIA (2013) and the July 18, 2022 drone survey to visualize the failure geometry and to calculate source and entrainment volumes. Pre-landslide elevation grid data was clipped along the extent of the eroded area to generate a 3D mesh of the landslide base. From the base, the contact between the old deposits and the landslides was inferred and depicted in the 3D geological models using polylines on multiple section planes parallel and perpendicular to the flow direction. From these models, the volumes of the source rock, the entrained debris, and the final deposit were calculated. Model outputs were cross-checked against field observations and mapped deposit extents to ensure consistency.

https://doi.org/10.5194/egusphere-2026-2543
Preprint. Discussion started: 22 June 2026

5 Results

5.1 Prolonged Rainfall, Floods, and Landslides in Leyte

Rainfall records indicate prolonged and intense precipitation between April 1 and April 13, 2022 (Fig. 2A), resulting from interacting tropical weather systems (Fig. 2B). A low pressure area (LPA) contained within the Intertropical Convergence Zone (ITCZ) traversed the Philippine Sea from April 2 to 6 and brought heavy rainfall to the southeastern Philippines. Flood and landslide events were recorded by April 5 (NDRRMC, 2022; Supplementary File 1). This LPA moved back to the Philippine Sea, and by April 7, the cumulative rainfall in the area had already exceeded 100mm, the average rainfall in Tacloban City for the month of April.

On April 8, 2022, 4 pm (GMT+8), another LPA formed east of Samar (10°30'N, 127°0'E) and brought in even more rainfall in the region. This system then developed into a Tropical Depression and was named Megi (Local Name: Agaton) by 5am (GMT+8) on April 9 (PAGASA, 2022). The next day, it intensified into a Tropical Storm. It then made landfall over Calicoan Island, Guiuan, Eastern Samar by 7:30 am (GMT+8) and slightly weakened by 11 pm (GMT+8) before its landfall over the eastern coast of Leyte. On April 11, by 8am (GMT+8), TS Megi weakened into a tropical depression while over San Pablo Bay, before it made landfall over Basey, Samar at 4 pm (GMT+8).

By April 11, rain had poured continuously on Leyte Island for almost four days (Fig. 2A) mainly due to the slow, meandering movement and stalling behavior of TS Megi over the Leyte-Samar Area (Fig. 2B, PAGASA, 2022; Supplementary File 1A). Most of the hazard incidents in the region were reported on April 10 and 11, including the major landslides in Kantagnos and Bunga in Baybay, Leyte, and the floods in Abuyog town proper. Abuyog MDRRMO noted that landslides also occurred in Barangays Bahay and Tib-o. By April 11, Barangay Pilar had been isolated due to the minor landslides along the road to Barangay Malaguicay (Supplemental File 1B).

5.2 Local geological and geomorphological context

Remote sensing analysis, UAV-derived DSM and orthophoto, and field observations show that the Pilar landslide originated from a steep, fault-cut volcanic ridge 590m SSW of Barangay Pilar (Fig. 3A). The ridge is characterized by steep slopes, narrow crests, deeply incised gullies, and a highly dissected surface morphology. These features were more defined in the post-landslide DSM (Fig. 3B), as the landslide had entrained source rocks, sediments, and vegetation from this ridge.

Field mapping identified prominent landslide scarps and arcuate failure surfaces upslope of the deposit fan (Fig. 3B). These features define the lateral and upslope boundaries of the source area. Multiple scarps of varying heights were observed both in the field and in the elevation difference map (Supplementary File 2C). Compared to the fully vegetated ridge in 2020 pre-landslide satellite imagery, freshly exposed soil and rock surfaces at the scarp face with sharp edges and minimally weathered textures are seen in the orthophoto (Fig.3A).

https://doi.org/10.5194/egusphere-2026-2543
Preprint. Discussion started: 22 June 2026

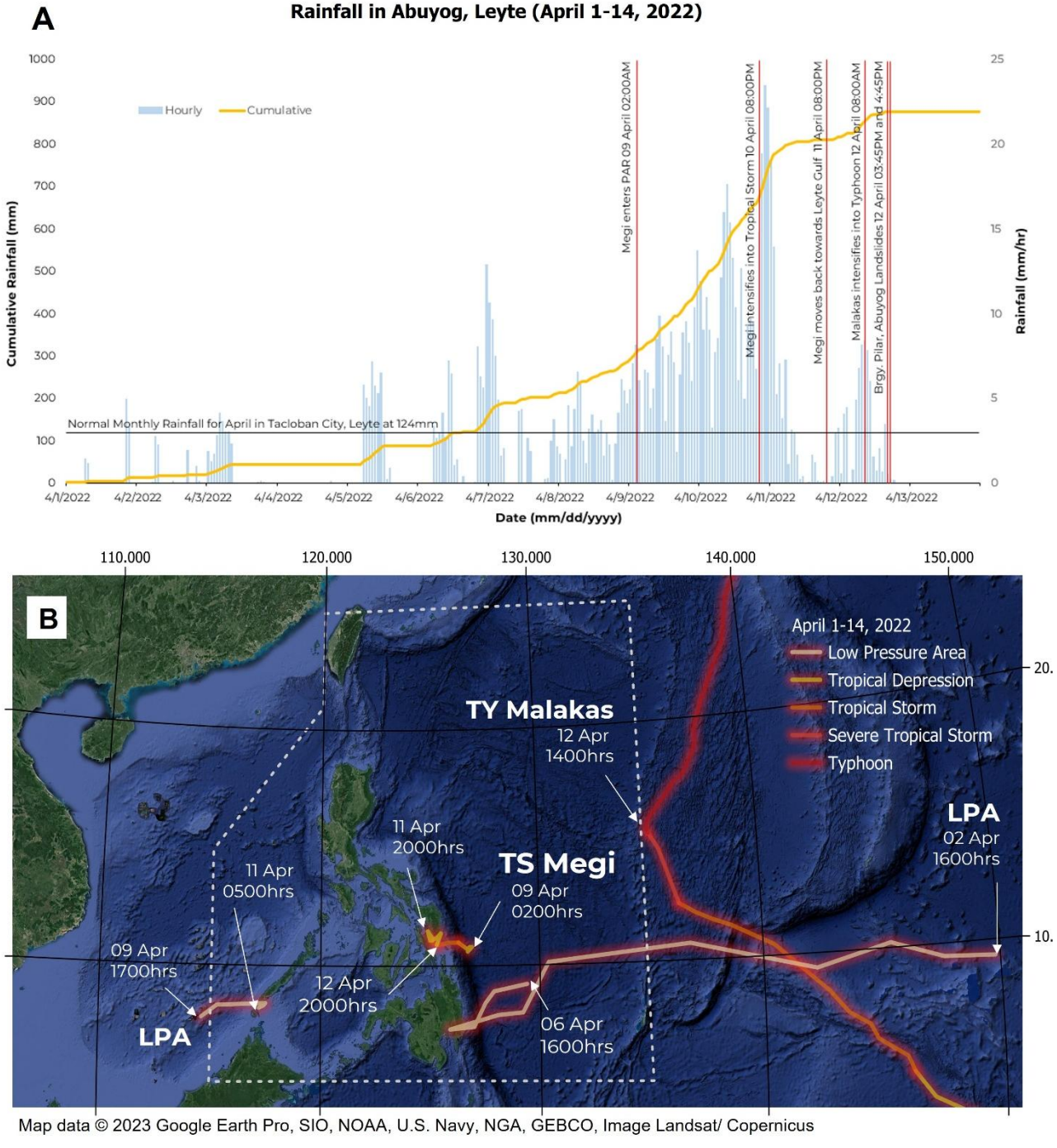

Figure 2: Rainfall brought by low pressure areas, Tropical Storm Megi (Agaton) and Typhoon Malakas (Basyang) on April 1-14, 2022. A) Hourly and cumulative rainfall time series in Abuyog, Leyte from April 1 to 14 (Data from JAXA, 2022). B) Tracks of the low pressure areas and tropical cyclones that affected the Philippines from April 1 to 12, 2022 (track data plotted from PAGASA, 2022; base satellite imagery from © 2023 Google Earth Pro, SIO, NOAA, U.S.Navy, NGA, GEBCO, Image Landsat/ Copernicus).

https://doi.org/10.5194/egusphere-2026-2543
Preprint. Discussion started: 22 June 2026

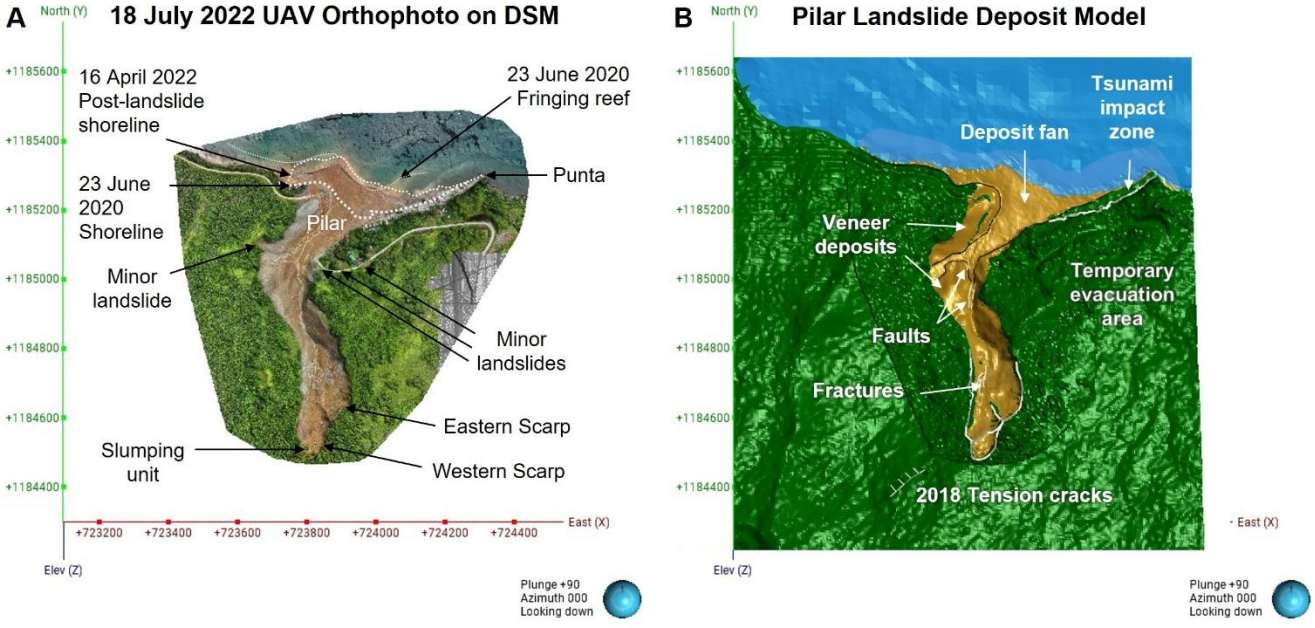

Figure 3: 3D Rendering of UAV and Field Survey Data. A) 18 July 2022 UAV Orthophoto on DSM. B) Pilar Landslide Deposit Model (Basemap elevation data from NAMRIA, 2013, rendered in Leapfrog Geo 2023.1).

The source area is underlain by poorly sorted gray to reddish-brown volcaniclastic deposits composed of angular to subangular clasts embedded in a sandy-silty matrix. Clasts range from gravel to boulder-sized. The landslide deposits are weakly consolidated and highly weathered. Saturated ground conditions, seepage zones, and localized ponding were observed along tension cracks and at the base of scarps. This major landslide scarps are 200m away, along the strike (N66°E) of the 100 meter-long, 5 cm to 20 cm wide tension cracks mapped in 2018 by the MGB Region VIII at 10° 42'27.61" N, 125° 2'39.54" E (Fig. 3B).

NNE-trending faults are also identified from the UAV imagery (Supplementary File 3). The linear structures abruptly cut the drainage pattern on the surface of the veneer deposits of the landslide. Verified on the ground at Station 6, near the apex of the deposit fan, this set of structures appears to extend southward, towards the edge of the western scarp. The deep incision of the channel runs parallel to these faults. A slickenside is noted on the surface of the outcrop at Station 6 (Supplementary File 2B).

5.3 Pilar Landslide Tsunami Events Chronology

Based on situational reports, video clips, and interviews with local government officials and eyewitnesses from Barangays Pilar, Malaguicay, and Bahay, the sequence of landslide and tsunami events on 12 April 2022 is reconstructed (Table 1).

https://doi.org/10.5194/egusphere-2026-2543
Preprint. Discussion started: 22 June 2026

230 **Table 1. Summary of eyewitness accounts and video-based observations of the Pilar landslide–tsunami sequence.**

Event Phase	Approx. Time	Process	Key Observations	Representative Quote	Source
Pre-failure	~14:00	Ground deformation	Cracks and slow slope movement; funnel-like deformation; stream blockage	"The slope already cracked and was slowly slipping… like a funnel."	Eyewitness (offshore fishermen)
DF1a	~15:00–16:00	Debris flow	Rapid collapse; highly saturated, thick flow; widespread burial	"Right after the burst… the village was covered by soil." "It was higher than electric poles and coconut trees…"	Eyewitness
			Fast-moving, wave-like flow with mixed debris	"It had waves as it flowed…" "like it was smoking...as it crawled down the slope"	Eyewitness
T1	As DF1a reached the sea	Tsunami waves	multiple waves; first clearer, later muddy with debris	"a churning motion, like a whirlpool formed in front of the landslide" "the landslide created something like a tidal wave… it caught me… the tsunami wave was enormous" "up to the 3rd floor or rooftop of a building" "The first wave was just water, the second had soil."	Eyewitness
		Coastal inundation	Repeated submergence; strong turbulence; debris transport	"I was rolled under the water… then another wave came."	Eyewitness + video
DF1b	Before T1 waves settled	Secondary failures	Smaller but closely spaced landslides	"Another landslide came… not as large as the first."	Eyewitness
Rescue arrival	~16:30-16:40	Response	Access by sea due to blocked roads	"We arrived around 4:30 or 4:35 to 4:40."	Eyewitness
DF2	~16:45	Debris flow	Visible downslope collapse; channelized flow; strong sound	"It sounded like an airplane… bursting from beneath..." "the coconut trees in the slopes were tumbling down; green at first as it moved down, then suddenly the green was gone, the trees were swallowed up."	Eyewitness + video
T2	As DF2 reached the sea	Tsunami waves	Smaller but energetic wave; disrupted rescue operations	"When the landslide hit the water… the wave returned and pushed toward the coast." "by 2 to 3-storey high waves"	Eyewitness + video

https://doi.org/10.5194/egusphere-2026-2543
Preprint. Discussion started: 22 June 2026

Prior to the main failure, signs of slope instability were already observed. Around 14:00 (GMT+8), residents offshore noted progressive deformation of the slope south of Pilar, describing visible cracking and slow downslope movement. At approximately the same time, residents in Pilar reported that a stream running through the village had ceased to flow, possibly due to upstream blockage by an earlier minor landslide along the road to Pilar (Fig. 3A).

Between approximately 15:00 and 16:00 (GMT+8), the first major landslide occurred. Residents consistently described becoming aware of the event through a sudden, loud sound ("pagputok") associated with rapid slope collapse. The failed mass transformed into a highly mobile debris flow (DF1) that traveled downslope toward the village. Eyewitnesses described the first landslide (DF1a) as waterlogged, fast-moving, and several meters thick, carrying a mixture of soil, rocks, and plant debris. The impact of the debris flow resulted in sudden widespread burial and destruction within Barangay Pilar.

Upon reaching the coast, DF1a generated a series of tsunami waves (T1) that reached adjacent barangays (Supplementary File 4 A-1). These waves occurred in rapid succession and were characterized by strong turbulence and increasing sediment load. The initial wave was followed by more debris-laden flows, consistent with continued mass entry into the coastal zone. The waves overtook residents who had fled toward the shoreline and caused extensive damage to coastal structures. The largest wave was associated with the initial debris-flow impact.

Within minutes of the first event, additional slope failures (DF1b) occurred. Although much smaller than the initial collapse (DF1a), these events were closely spaced in time. Rescue operations began shortly after the initial event, with responders arriving by sea at 16:30 (GMT +8) due to blocked access roads. At approximately 16:45 (GMT+8), a second major landslide (DF2) occurred during ongoing rescue efforts. This event, captured on video, followed a similar pathway but was more confined within the previously incised channel.

Upon reaching the coast, DF2 generated a second tsunami (T2). Although smaller than the first, the waves remained significant, with sufficient energy to disrupt rescue boats and strip vegetation along the shoreline. Unlike T1, the second tsunami did not propagate as far alongshore but still posed a substantial hazard in the near field.

Overall, the Pilar event consisted of at least two major debris flow phases and corresponding tsunami wave trains occurring within a span of less than two hours. The rapid succession of landslide and tsunami events highlights the cascading nature of the hazard and the potential for multiple, temporally clustered impacts in rainfall-induced landslide–tsunami systems.

https://doi.org/10.5194/egusphere-2026-2543
Preprint. Discussion started: 22 June 2026

5.4 Landslide Morphology, Velocity, and Volumes

5.4.1 Initiation Zone

Pilar landslides originated from the slopes of an old and highly weathered volcanic edifice (Fig. 4A). Although two distinct 100-meter-wide, 30-meter-deep scarps are immediately recognizable from satellite images and in the field, both have landslide units obscuring their cross-cutting relationship; hence, the sequence of slope failure is not yet certain.

Satellite and drone orthophoto of the western scarp revealed that the slump head had moved within three months after the event. The western crown had split into two units parallel to the scarp. The risk of landslides in the area remained. This prompted us to limit our stay in the debris field because the materials in the source area were still moving.

Soil, boulders, and plant debris from both scarps drain into a 145-meter-wide depression where Step 1(St1) accumulated (Fig. 4A). Both sides of this bowl-shaped feature are lined by muddy veneer deposits left by DF1(gray) and DF2(brown) indicating that both flows ran up the flanks of this depression as they incised 20-30m deeper through the pre-existing topography.

Drone images show that the Initiation Zone is comprised of light gray source rock that becomes reddish (oxidized) and weathered into brown soil towards higher elevation. Near the top of the soil mantle is a distinct boulder-rich layer upon which vegetation was anchored, as seen both on the slumping units and the scarp. DSM differencing (Supplementary File 2C) indicates scarp depths exceeding 30 m in areas affected by successive flows, with total mobilized volumes on the order of 10^5-$10^6 m^3$.

Based on slightly different descriptions of eyewitnesses, we created three models to depict the possible sequence and initiation volumes of the slope failures (Fig. 5 and Table 2). Model A assumes a top-down failure, where the western crown failed first, given its higher elevation and steeper slope. This also makes it visible to the fishermen offshore of Pilar, who described it to be slowly moving on April 12, 2 pm. This model estimates around 3.4 x 10^5 m^3 of initial volume from the western scarp, which entrained around 4.9 x 10^5 m^3 more, followed by 1.9 x 10^5 m^3 second event from the eastern scarp. Months later, these are followed by slumping (S) again in the western scarp.

In Models B and C, failure initiates at the eastern crown, carving a large bowl-shaped depression within the gray source rock, followed by subsequent failures of the soil-rich units upslope. Model B assumes a single slope failure of approximately 3.5 × 10^5 m^3 that transformed into DF1, which then continued downslope and generated T1. During transport, this flow is inferred

https://doi.org/10.5194/egusphere-2026-2543
Preprint. Discussion started: 22 June 2026

to have entrained an additional ~5.0 × 10^5 m^3 of material. This model provides a plausible explanation for the observed differences in color and composition between DF1 and DF2 deposits.

285 In contrast, Model C reflects eyewitness accounts describing two closely spaced landslides (DF1a and DF1b) prior to the arrival of rescuers, with the first event having a substantially larger volume (~2.8 × 10^5 m^3) than the second (~6.7 × 10^4 m^3). A third landslide (~1.6 × 10^5 m^3) then occurred during ongoing search and rescue operations, generating T2.

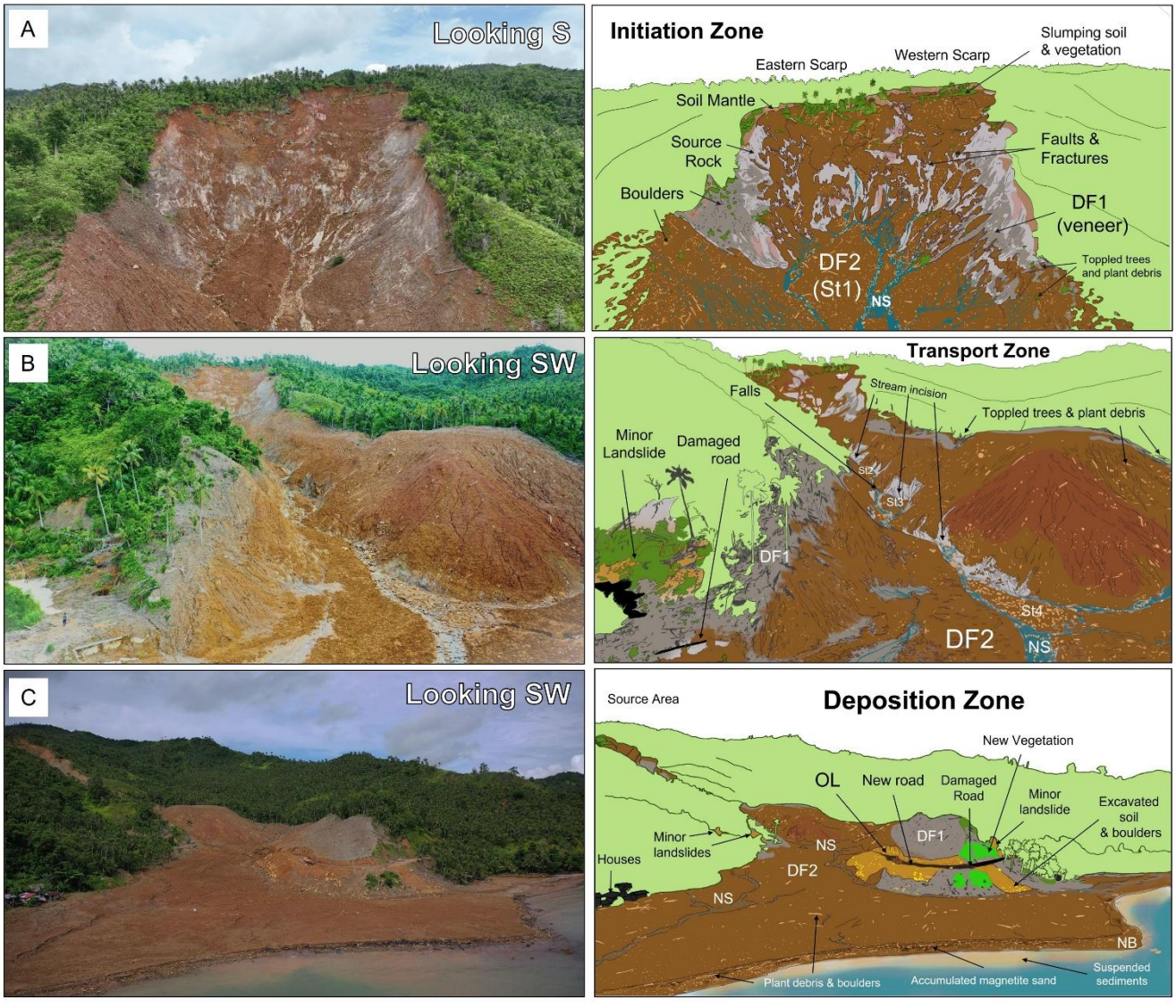

Figure 4:Geomorphological features of the Pilar Study Area interpreted from UAV and field survey data. A) Initiation Zone, B)
290 **Transport Zone, and C) Deposition Zone. On the left side are the drone photos by A. Bermas on July 18, 2022, while the right side highlights the interpretation of deposits. (OL– old landslide deposit; DF – Debris flow deposit; St – step deposit; NS – new stream; NB – new beach deposits).**

https://doi.org/10.5194/egusphere-2026-2543
Preprint. Discussion started: 22 June 2026

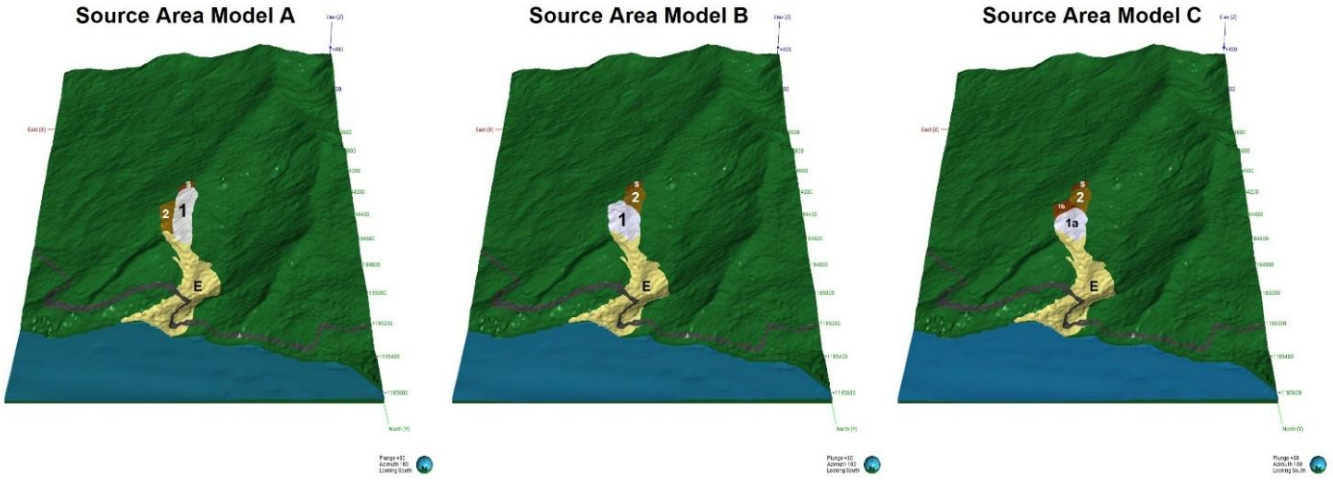

Figure 5: Source area models of the Pilar landslide–tsunami cascade. A) Top-down failure, plus slump. B) Bottom-failure initiated, plus slump. C) Progressive Bottom-failure initiated. (1: Landslide 1; 2: Landslide 2; S: Slumping Unit; E: Entrained Volume; Basemap elevation data from NAMRIA, 2013; rendered in Leapfrog Geo 2023.1)

Table 2: Calculated volumes from Leapfrog Geo 3D Models of the Pilar Landslides

Unit	Volume (m^3) (Models at 5m resolution)		
	Source Model A	Source Model B	Source Model C
DF1 Source (1)	340,420	350,440	283,170
			66,854
DF2 Source (2)	187,510	163,640	163,870
Slumping unit (S)	35,647	36,524	36,524
Entrained (E)	490,960	501,150	501,150
DF1 (1+ E)	831,380	851,590	784,320
Debris flow source (1+2)	527,930	514,080	447,040
Source Volume (1+2 + S)	563,577	550,604	550,418
Total volume (1+2+S+E)	1,054,537	1,051,754	1,051,568
Comparison with deposit model volume (555,758 m^3)			
Without entrained volume	1.41%	0.93%	0.96%
With entrained volume	89.75%	89.25%	89.21%

While these models are currently being evaluated using landslide–tsunami simulations, field evidence and mapped impact patterns consistently indicate that the first landslide had the highest momentum, resulting from a combination of greater source volume, entrainment, and/or higher velocity. Remote sensing observations further suggest the presence of a residual slumping unit at the western scarp.

https://doi.org/10.5194/egusphere-2026-2543
Preprint. Discussion started: 22 June 2026

Among the three conceptual models, Model C is considered the most consistent with the available field, video, and eyewitness evidence. It accounts for multiple closely spaced debris-flow events preceding and accompanying tsunami generation, as indicated by the temporal clustering of slope failures and successive wave impacts. The distinction in deposit characteristics between DF1 and DF2, together with the documented event sequence, supports a progressive failure mechanism rather than a single or strictly top-down collapse.

5.4.2 Transport Zone

Field observations at Stations 1-10 (Fig. 6) provided insight into the transport of the debris flows. As shown in Fig.6B and C, DF1 incised 20m deeper through the pre-existing stream valley, scraped off vegetation, and exposed pre-existing volcanic rocks and NNE-trending faults. It also ran up over the ridge behind S7 (Fig. 6A), cut off the road, and left a 20-50cm thick levee deposit over the damaged road (Fig. 6B).

On the opposite edge of the flow, DF1 ran up the ridge 17m northwest of S4 and S5 (Fig. 6C; DF1 flow direction is marked by dashed lines). Using the UAV DSM, a superelevation height of 23.13m was measured from DF 1 levee deposits at S7 and the veneer of tuffaceous gray matrix on the ridge behind S5. With a flow width of 126.63m, and a radius of curvature of 165.74m, we estimate that DF1 had a velocity of 17.23 m/s at this bend. At S4, DF1 deformed the highly weathered matrix of the old landslide deposits (OL), leaving a flame structure at their contact (Fig. 6E). DF1 flowed over this ridge and then spilled over to S1-S3 (Fig. 6C). At S3, DF1 left a maximum of 25cm-thick deposit while at S2, it was about 20-30cm thick. At S1 (Fig. 6D), at least 40cm thick-sediments and debris are accumulated near the root of the coconut trees. Runup of 1.8m was measured from the scratches on the trees, indicating a velocity of around 5.9m/s at S1.

The debris flow 2 (DF2) on the other hand, was confined within the valley incised by DF1 (Fig. 6A; DF2 flow directions indicated by solid white arrows). The soil-rich deposit filled Steps 1 to 4 (Fig. 4B) and left a muddy veneer on the valley and ridges on its path (Fig. 6A and B). In the inner bend, deposit sequences at S7 and S8 (Fig. 6B) show that DF2 eroded DF1 deposits in the valley, and left a thin layer on the surface of DF1 levee deposit. In the outer bend, superelevation reached about 7.95m between S7 and S5 (Fig. 6C), indicating a velocity of about 12.5m/s. Notably, an inverted coconut tree is seen piercing through the DF2 muddy veneer and the indurated OL deposits at S4, displaying the power of DF2 at this point.

Upon impact, DF2 meandered back to the valley, leaving only a muddy veneer on the ridge. The impact of DF2 on the ridge was also captured on video (frames highlighted in Fig. 7). The flow is seen to carry sediments suspended in the air behind the flow front. The dust cloud appeared compressed as the flow hit the ridge then it spread as DF2 deposited over DF1 at the coast.

https://doi.org/10.5194/egusphere-2026-2543
Preprint. Discussion started: 22 June 2026

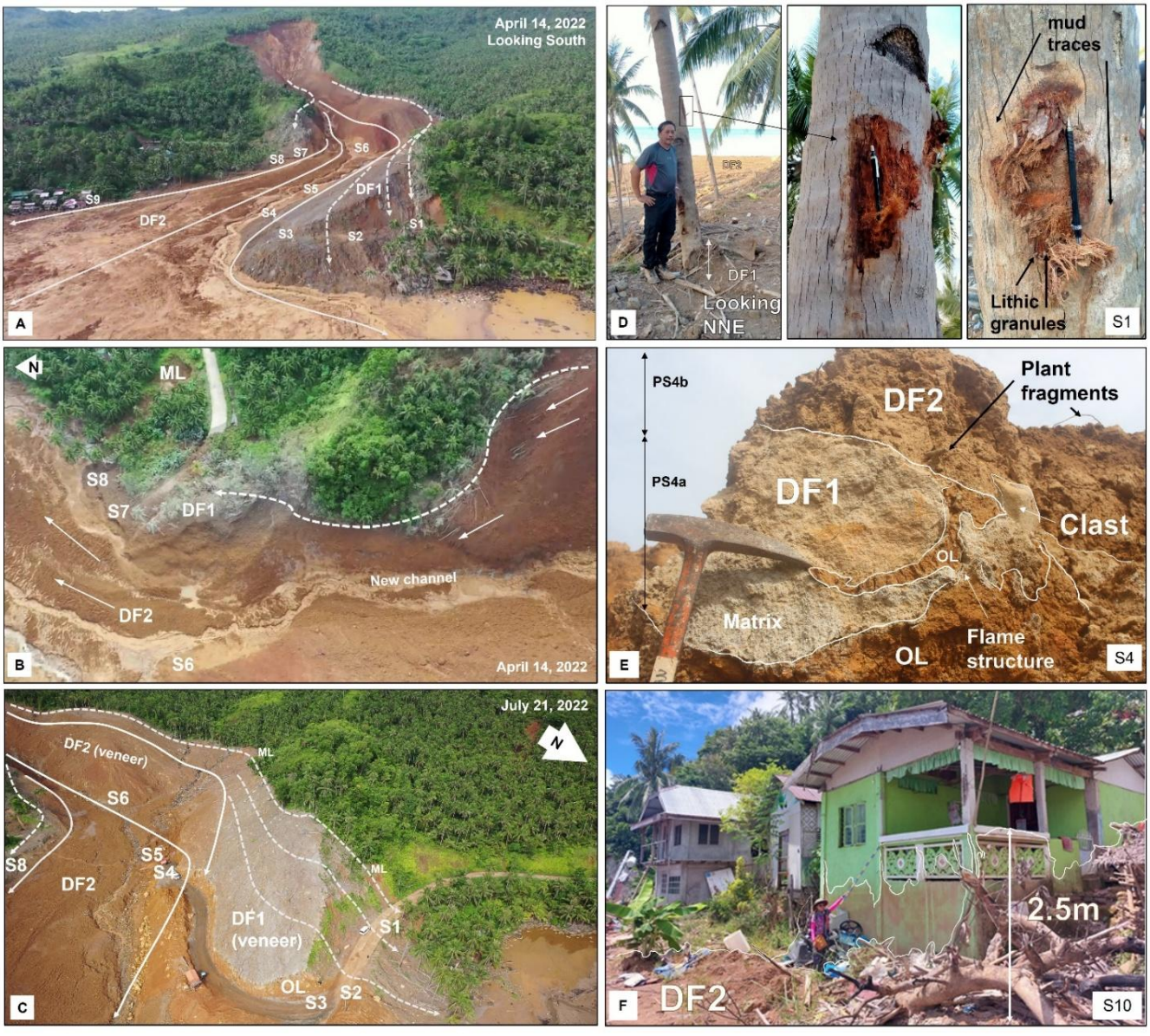

Figure 6: Debris flow directions based on the orientation of toppled trees and depositional structures (DF1 dashed; DF2 solid arrows). A) April 14, 2022 drone footage posted by GPM TV Philippines via Youtube. Field survey stations in July 2022 are marked (S1 to S9). B) New channel formed after DF1 & DF2. C) Superelevation marks on the western extent of DF1 & DF2 on a ridge underlain by an older landslide deposit (OL). D) The runup height (1.8m) of DF1 as indicated by scratches on coconut trees along the main road at S1. E) The contact between OL, DF1 and DF2 along the new roadcut, where soft-sediment deformation (flame structure) was observed at the contact of DF1 with OL at S4. F) House at S10, along the edge of DF2 deposits where debris flow runup of 2.5m was observed.

https://doi.org/10.5194/egusphere-2026-2543
Preprint. Discussion started: 22 June 2026

5.4.3 Deposition Zone

Comparison of the 1956 topographic map (NAMRIA, 1956), the 2012 DEM, the 2016-2021 historical satellite imagery of Google Earth, and the 2022 drone DSM from this study indicates that the small bay north of Barangay Pilar was transformed by the landslides into a delta that takes the shape of the fringing coral reef (Fig. 3D). April 16, 2022 satellite image shows that the landslide advanced the shore by as much as 95 m (parallel to the new channel) and expanded the coastal area by 2.6 x 10^4 m^2.

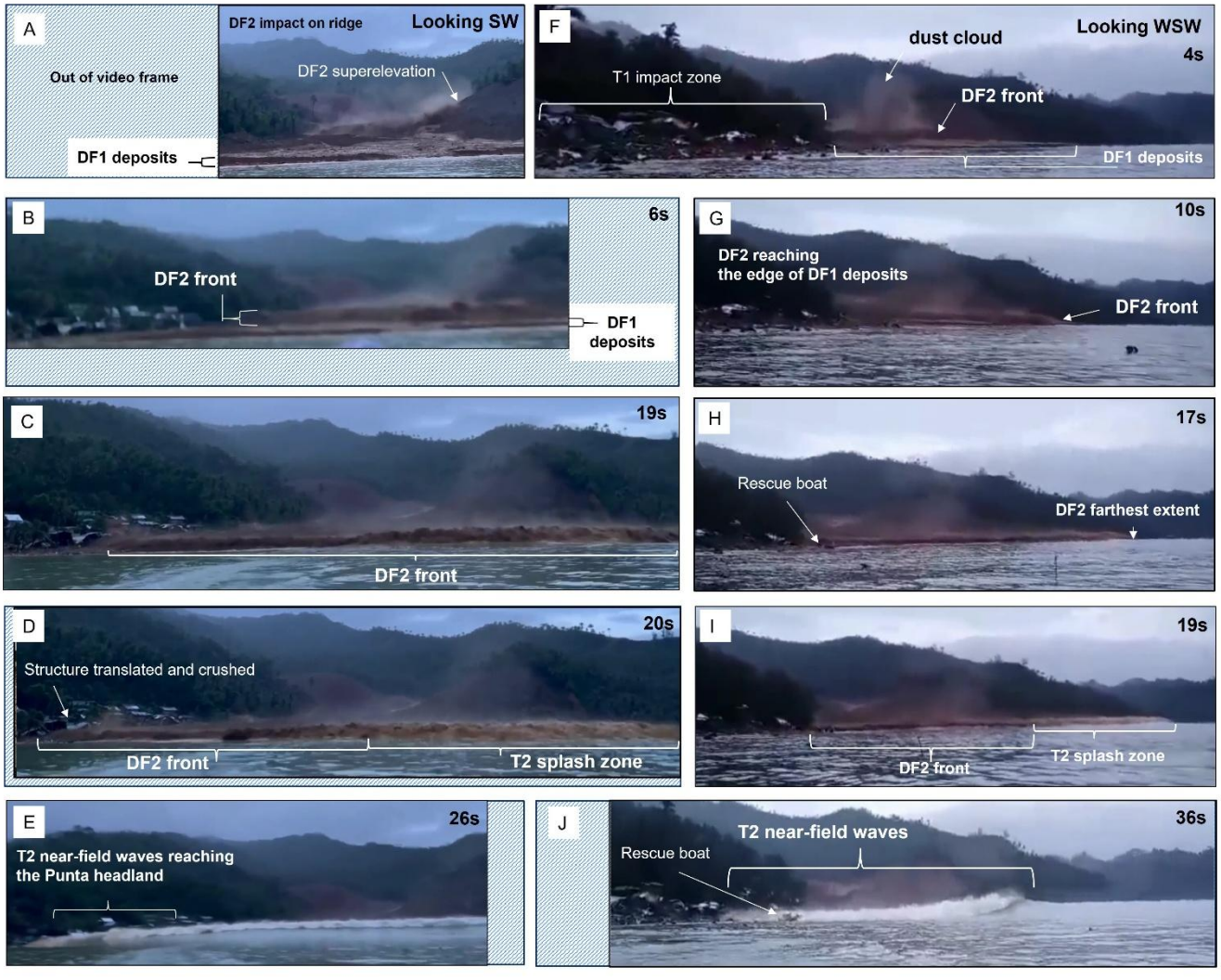

Figure 7: Frames from videos taken by rescuers at Pilar as DF2 flowed over DF1, reached the shore and generated Tsunami 2 (T2) (A-E: looking southwest c/o PDRRMO, 2022; F-J: looking west-southwest c/o BFP Region VIII, 2022).

https://doi.org/10.5194/egusphere-2026-2543
Preprint. Discussion started: 22 June 2026

The onshore exposure of the debris fan spans around 5.1 x 10^4 m^2. Its maximum thickness could not be measured, but we estimate the new delta to be between 2 to 6 m thick. This is based on the bathymetry data of the near-shore areas (NAMRIA, 1956), which had a depth of 3m. The auger we used was 2m long, and we could not reach the underlying ground nor the contact between DF1 and DF2. In addition, based on the videos of DF2 (Fig. 7), we estimate that the surface of the DF1 fan deposit is at least a meter above sea level before it was buried by the succeeding deposits. 3D post-landslide model (Fig.3B) estimates a total deposit volume (from source area to the offshore debris front) be around 5.6 x 10^5 m^3.

The deposits of DF1 and DF2 were distinguished by their color, composition and stratigraphic relationships in outcrops in Stations 2, 4, 7 & 8 (Fig. 6A). As shown in Fig. 4, DF1 deposited as a gently sloping debris fan with levee and veneer deposits on the flanks of the valley where Barangay Pilar used to be. Its destructive power was demonstrated by the translation of the Barangay Gymnasium 185 m downstream (Fig. 7C). This structure and the debris fan deposits of DF1 were almost fully covered by DF2; what remained exposed were the levee and veneer deposits of DF1.

In drone images, DF1 sites are characteristically grayish from afar. Field and hand samples show that DF1 deposit is composed of buff to light grey pebble to cobble-sized, angular to rounded, elongated to spherical clasts set in gray to light brown tuffaceous matrix. These clasts are lightweight and often crumble into chips that are also magnetic. Some clasts exhibit white to grey, altered plagioclase crystals set in grey groundmass. These characteristics point to an altered porphyritic andesite source rock (Supplementary File 5A).

Sediment samples of DF1 are poorly to very poorly-sorted and have median grain sizes (D50, ϕ) between 0.125 to -1.444 (Fig. 8C). Sieved granules (2-4mm) of DF1 are composed of gray, greenish grey, yellowish grey, white, dark brown, red, peach and black sub-angular to rounded, low to moderately spherical grains coated by grey ash. 1-2.5% of the fine sand particles are magnetic, while at medium sand size, slightly magnetic grains make up 60-90%. Plant fragments are also noted in all samples. DF2 deposits, on the other hand, appear brown and muddy from afar. At S9 and S10 (Fig. 6F), DF2 deposited on infrastructure debris and tree trunks onto the houses. Mud ran up to 3m at S9 and 2.5m at S10, suggesting the DF2 velocity at this edge of the fan to be around 7.0 – 7.7m/s. Whereas, from the videos (Fig. 7), using multiple markers on the deposit fan, we estimate DF2 velocities between 11.29 and 24.71 m/s.

Upon closer examination of the DF2 debris fan deposits (Fig. 8A and B), we identified clasts to be subrounded to rounded cobbles and boulders of porphyritic andesite often encrusted by yellowish clayey but indurated alteration and sub-angular to subrounded red or gray, altered andesite cobbles (Supplementary File 5B and C). These clasts are notably similar to the boulders seen in the source area and the OL deposits between S3 and S4 (Supplementary File 5D and E). This lithology also makes up the granules and pebbles in the matrix (Fig. 8B). Auger samples of DF2 are poorly to very poorly-sorted and have median grain sizes (D50, ϕ) greater than 4 (Fig. 8C). Sieved granule samples are composed of angular to subangular grains with medium to low sphericity. Grains are cream, yellowish to reddish brown in color. Some lithic grains are white with dark

https://doi.org/10.5194/egusphere-2026-2543
Preprint. Discussion started: 22 June 2026

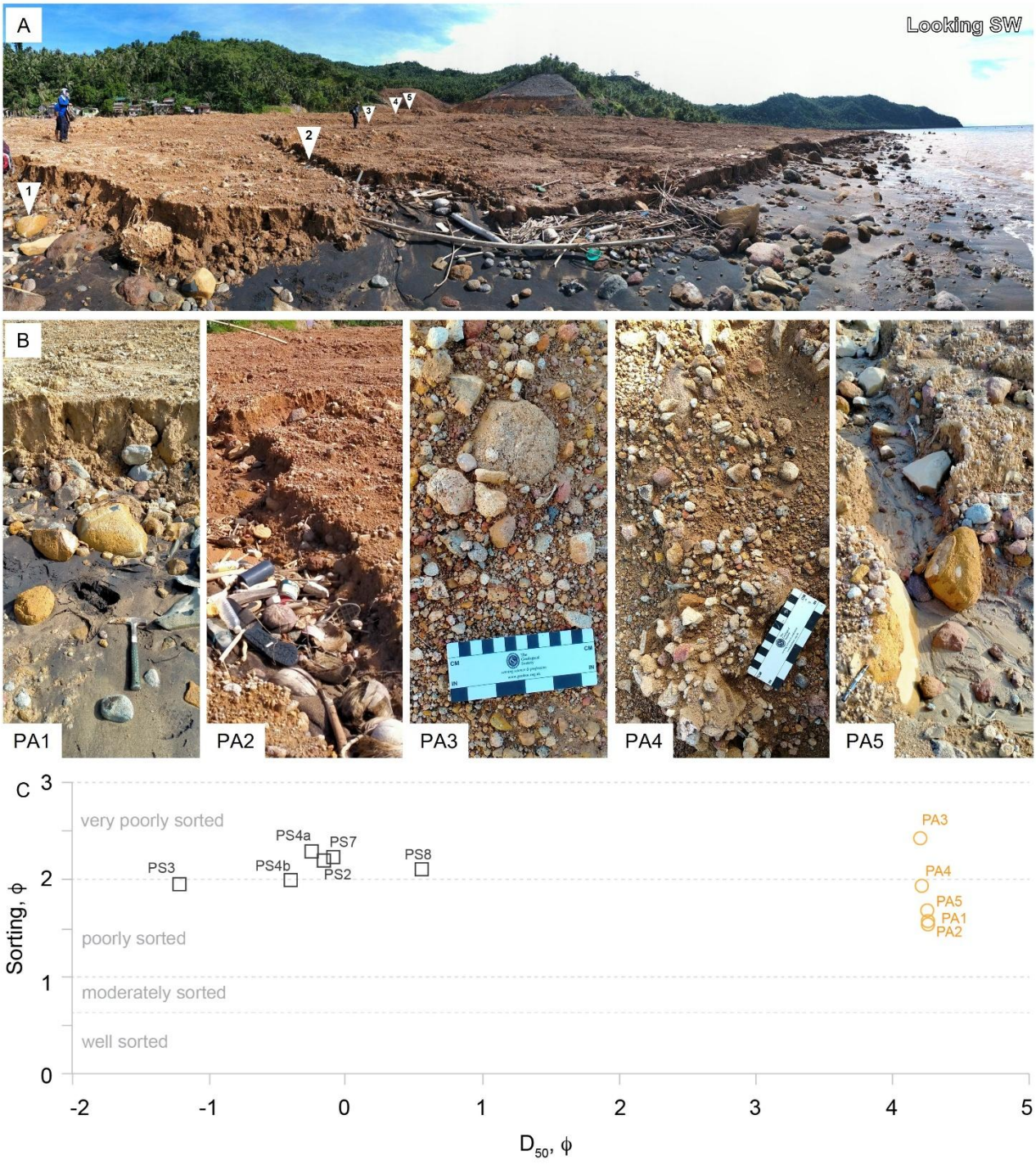

Figure 8: Auger Sampling Stations (A1 to A5). A) Panoramic shot at the July 19, 2022 coast of Pilar; inverted triangles marking the Auger Sampling points. B) Surface of DF2 sample sites. C) Sediment Analysis of DF1 (gray squares) and DF2 (brown circles) samples.

https://doi.org/10.5194/egusphere-2026-2543
Preprint. Discussion started: 22 June 2026

minerals. Plagioclase, charcoal grains and plant fragments are also present. Lithic grains have magnetic components, the proportion of which increases to 80% at very fine sand size.

By July 2022, DF2 deposits had been scoured deeper by new channels (Fig. 4C). In places, especially near the tail of the fan (Fig. 4B), reworked DF1 deposits are seen in the channels and puddles over the DF2 debris fan (Fig.8B PA5). Along the coast, DF2 is overlain by beach deposits that are composed mostly of black magnetite sand and a lower concentration of brown mud (Figs. 4C and 8A). Personal effects (e.g., water bottles, rubber soles of footwear; Fig. 8A and B), plant debris, and assorted rounded boulders are also concentrated along the shore. As shown in Fig.3 and Supplementary File 6, the debris fan has since transformed into a wave-dominated delta.

5.5 Tsunami observations

Evidence, including eyewitness accounts, remnant debris, surface feature alteration, and video recording, indicates tsunami runup heights ranging from 0.82 MASL to as high as 11.67 MASL (Fig. 9). All eyewitnesses in Pilar described DF1 as the one that caused the biggest wave (T1). As DF1 curved at the ridge north of S4-S5, its momentum upon reaching the water caused the impact of T1 to be concentrated on the eastern side of Pilar coast. T1 travelled 2.1 km to the east, reaching Malaguicay, running up to 3 MASL and 800m to the west towards Bahay, reaching 0.82 MASL.

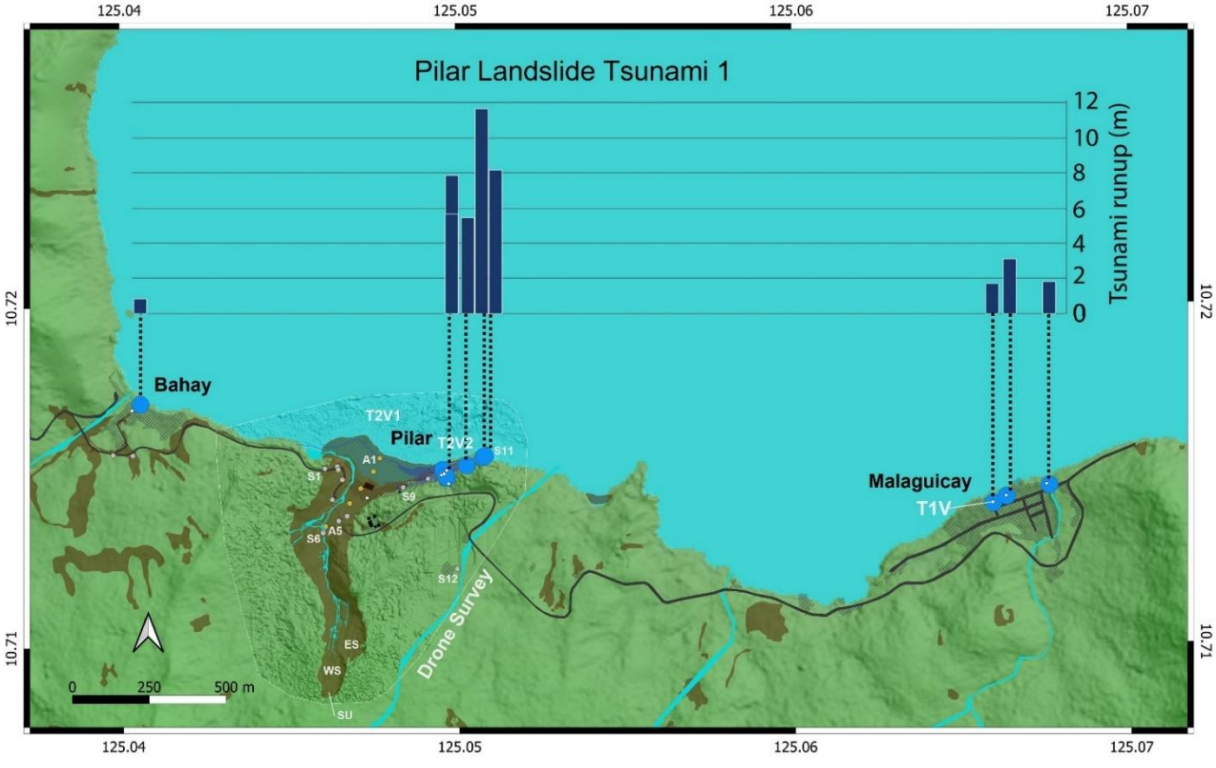

Figure 9: Measured tsunami runup heights of Pilar Landslide Tsunami 1 in Barangays Bahay, Pilar and Malaguicay (Elevation data from NAMRIA, 2013).

https://doi.org/10.5194/egusphere-2026-2543
Preprint. Discussion started: 22 June 2026

5.5.1 Splash Zone

Based on the previous topography and bathymetry, T1 splash zone would have been within the small embayment of Barangay Pilar. There were no videos of T1 in Pilar to confirm the churning motion described by eyewitnesses, but videos of DF2 reaching the waters beyond DF1 deposits (Fig. 7D and I) showed a turbulent splash zone at the front of DF2. This uprush lasted about three seconds before the wave spread to the coast of Pilar (Fig.9D).

5.5.2 Near Field Waves

Field survey revealed that the highest runup elevation (11.67m) was at the Punta headlands (S11) near the Pilar Barangay Center, where the residential and commercial areas were previously situated. The tsunami impact zone (9,008 m^2) spans around 335m parallel to the wrackline and up to 55m perpendicular to the shore by July 18, 2022 (Fig. 10A). This area (from S10 to S11) which used to be filled with around 50 houses, was reduced to the ground. All single-storey concrete and wooden structures near the shore were shattered by T1. Second-floor structures remained semi-intact but were translated by the waves. Measurements from the remaining second-floor structure and the foundation of the house (Fig. 10B and C; house with yellow walls, red roof, green columns) indicate that the southwest column was translated by 17.1 m, the southeast column by 11.5m; the long axis of second-floor structure has rotated by around 67° from its original orientation.

After the T1 slammed the coastal Pilar area, the waves spread to the east, towards Malaguicay. A resident there documented the arrival of the first tsunami wave (T1a, Supplementary file 4). This wave peaked 6 seconds later, then receded, until a second wave (T1b) came by the 18th second. The sea continued to recede until 35 seconds later, revealing the debris left at the shore of the barangay. A third wave (T1c) was also recorded coming in later on a second video but it was weak and was not as large as T1a. Turbid water from the previous waves was still evident in these frames. It also showed multiple empty boats carried out into the sea by T1.

Field measurements at this station where the videos were taken, indicates that T1 inundated up to 9m inland running up 1.8-3 MASL (Supplementary file 4J). In the easternmost station in Malaguicay, this wave run up to 1.9m, inundating up to 50m from the shore up a small river, bringing in debris and small fishing boats slamming onto houses. A house tilted by 11° due to the slamming of the boats on its coastal side (Supplementary file 4L). Measurement along the coast of Barangay Bahay indicates that the near-field waves runup on the western side was less than a meter (Fig.9). No boat damage was reported on this side.

Videos of T2 (Fig. 7D, E, I and J) showed its wave spreading from the splash zone towards the coast. The near-field wave appeared white and had a rolling motion. Calculating based on the distance of the DF2 front to Punta (425m) and the 37 seconds that it took the wave to travel this distance, we estimate the near-field wave of T2 to have a velocity of 11.48 m/s. T2 was not reported to have reached Barangay Malaguicay.

https://doi.org/10.5194/egusphere-2026-2543
Preprint. Discussion started: 22 June 2026

Figure 10: Landslide-Tsunami impact in Pilar. A) Extent of the tsunami impact zone. The white rectangle marks the extent of the next photo. Blue arrow shows the displacement of the Barangay gym. B) UAV photo of the tsunami debris (TD) field. The dashed white rectangles outline the red-roofed house and its foundation. Blue arrow indicate the displacement direction of its southern corners. C) Destruction and displacement of structures caused by the tsunami (T1) as seen from the ground.

https://doi.org/10.5194/egusphere-2026-2543
Preprint. Discussion started: 22 June 2026

6. Discussion

6.1 Landslide initiation and preconditioning factors

The Pilar event provides a rare, well-constrained example of a rainfall-triggered landslide–tsunami cascade in a tropical coastal setting. The results indicate that tsunami generation was governed primarily by high-momentum debris-flow impact, controlled by a combination of elevated flow velocities and short source-to-shore distances. These findings emphasize that dynamic flow properties, rather than landslide volume alone, play a critical role in determining tsunamigenic potential in near-field settings. In this context, the Pilar case extends existing models of landslide-generated tsunamis by demonstrating that rainfall-triggered debris flows in steep volcanic terrains can produce impact conditions comparable to those observed in larger subaerial or volcanic collapse events.

In addition to the proximity of the source area to the known NW-SE striking Central Leyte segment of the Philippine Fault (9.7km to the SW, Fig. 1C), we discovered NNE-trending faults upon which the Pilar debris flows incised through and where new falls and channels now flow through (Fig. 3C and 4B, Supplementary File 2). These have likely contributed to structural weakening of the slope through fault-related fracturing and enhanced permeability, as observed in other tectonically active volcanic regions (Tsutsumi and Perez 2013; Lagmay et al., 2003). Although no strong ground shaking coincided with the main failure, a shallow earthquake recorded one day prior to the disaster may have further destabilized critically stressed slopes, a phenomenon previously documented in rainfall–earthquake coupled landslide triggering (e.g., Sassa et al., 2007; Qu et al., 2023).

Around 750 landslides and/or erosional features were identified from the April 16, 2022 Google Earth Historical Imagery in the vicinity of Abuyog (Latitude: 10°37'20.00" N - 10°43'40.00" N, Longitude: 124°53'0.00"E - 125°6'45.00"E). Most of these landcover changes were identified in the eastern mountains of Abuyog, in the terrain classified “undifferentiated volcanics” by Sajona et al (1997) and on the ridges near the PFZ west of Abuyog (Fig.1C and Supplementary File 1). Around 33 of these are also reported by MGB (2022) for the onsite municipal assessment requested by the local government; six of which blocked the way to Barangay Pilar. Eleven of these also reached the coast, but only the Pilar Landslides were reported to have caused tsunamis. Several landslides of varying sizes were already visible along the road and bays approaching Barangay Pilar. Landscapes exhibiting early warning signs of possible impending landslides such as creeping trees and tension cracks in the soil were also found along road cuts and streams (Supplementary File 1). However, not all of these were extensively studied due to safety concerns.

Approximately 88 houses/buildings were affected in the approximately 13 hectares of land in Barangay Pilar (DOST-ASTI and PhilSA map, 2022). On-site, it was documented that the majority of Barangay Pilar was wiped out by the landslide with no buildings and vegetation left standing. During the inspection of this study on July 18, 2022, the area was filled with loose soil mixed with water and debris such as organic materials and scraps from infrastructures. The terrain is also constantly and

https://doi.org/10.5194/egusphere-2026-2543
Preprint. Discussion started: 22 June 2026

rapidly being reshaped as a response to the stream flow and weather. For instance, the soil in the barangay became more loose, wet, and unstable following intense rainfall on the eve of July 18. It was noted that the area is very susceptible to reworking and instability, evolving every day as a response to external factors. The Department of Public Works and Highways (DPWH) was already working on clearance operations during the time of the fieldwork. The road has since been reconstructed to restore access to the easternmost barangays of Abuyog. By 2025, vegetation in this area has partly recovered as well (Supplementary File 5). However, Pilar has since been abandoned; the whole community had to resettle in another location.

6.2 Transformation from slope failure to debris flow

Following initiation at elevations exceeding 200 m above mean sea level, the failed mass rapidly transformed into a highly mobile debris flow. Such transformations are common in saturated volcaniclastics, where excess pore-water pressure and entrainment of additional material would lead to flow-like behaviour and high mobility (Delcamp et al., 2016; Iverson et al., 1997; Iverson, 2005; Hungr et al., 2014).

UAV-derived DSMs and field observations indicate deep incision along the transport corridor, with scarp depths exceeding 30 m in areas affected by successive flows. At least two distinct debris flow events were identified based on stratigraphic relationships, deposit characteristics, and video analysis. The occurrence of multiple debris flows within a short time window is consistent with observations from other rainfall-induced landslide disasters, where partial slope failures progressively evolve into larger mass movements as rainfall persists or drainage conditions change (Jakob and Hungr, 2005; Highland and Bobrowsky, 2008).

Source Area Models A, B, and C have minimal difference (<±1.5%) in the calculation of the total initial source volume (Tab. 1: 1+2+ S) and the Total Deposit Volume. But if we add the entrained volume, total volume displaced becomes ~89% larger than the estimate from the deposit model derived from the post-landslide DSM. Possible sources of these discrepancies may be attributed to (1) compaction of the deposit during the three months prior to the UAV survey, (2) assumed vegetation thickness, (3) unknown undersea extent of deposits, and (4) outdated bathymetry data.

6.3 Landslide–tsunami coupling mechanism

The Pilar event represents a rare, well-documented sequence of rainfall-induced, subaerial landslides directly generating tsunamis. Landslide-generated tsunamis differ fundamentally from earthquake-generated tsunamis in that wave generation is impulsive, localized, and strongly dependent on landslide volume, velocity, and entry geometry (Okal and Synolakis 2004; Løvholt et al., 2015). In Pilar, at least one major debris-flow event with an estimated mobilized volume on the order of ~10^5 m^3 entered the coastal zone at velocities of ≥17m/s, producing tsunami waves with run-up heights reaching up to ~11.7 m above mean sea level.

https://doi.org/10.5194/egusphere-2026-2543
Preprint. Discussion started: 22 June 2026

A first-order description of the landslide–tsunami coupling can be expressed in terms of the Froude number (Eq. 3):

$$Fr = \frac{v}{\sqrt{gh}} \quad (3)$$

where v is the landslide velocity, g is gravitational acceleration, and h is the local water depth. Using observed debris-flow velocities near deposition and an estimated nearshore water depth of ~3 m based on available bathymetric data, the corresponding Froude number is on the order of ~1.29-4.61. This indicates strongly supercritical flow conditions, consistent with highly impulsive wave generation observed in both experimental and field studies (Fritz et al., 2004; Heller and Hager, 2010). A simple sensitivity check using nearshore depths that range from ~2–5 m based on the bathymetric map, yields Froude numbers of around ~1.00-5.64, confirming that the flow remains supercritical across a range of depth estimates. While these values are subject to uncertainty in nearshore depth and flow properties, they support the interpretation that the Pilar tsunami was generated under high-momentum impact conditions.

This interpretation is consistent with established scaling relationships, in which impact momentum—controlled by velocity and effective mass—plays a primary role in governing near-field wave generation. In this context, the Pilar case illustrates how relatively moderate-volume events can still produce substantial run-up when velocities are high, and the distance between source and shoreline is minimal.

Despite the absence of strong basin confinement, tsunami run-up heights in Pilar reached ~11.7 m above mean sea level. This can be attributed to the combination of high debris-flow velocity, substantial entrained volume, and the very short distance between the landslide source and shoreline, which limited energy dissipation before impact. In addition, local coastal configuration, including a bending landslide path due to adjacent headlands, and a semi-enclosed embayment likely contributed to partial wave focusing, as suggested by the observed asymmetry in run-up heights, with greater impact concentrated along the eastern sector of Barangay Pilar. Although the Pilar coastline is not strongly confined, these observations indicate that even modest coastal irregularities may influence wave amplification and spatial variability of run-up in near-field settings.

Comparison with well-documented global landslide–tsunami events provides further context for interpreting the Pilar case (Tab. 3). The 1958 Lituya Bay landslide represents an extreme example, where a ~3× 10^7 m³ rockslide impacting a confined fjord generated a maximum run-up of 524 m due to strong geometric amplification (Miller, 1960). Similarly, the 1963 Vajont Dam disaster involved a much larger (~2.70 × 10^8 m³) slope failure into a narrow artificial reservoir, producing run-up heights exceeding 200 m, strongly influenced by a paleo slide and a confined basin configuration (Panizzo et al, 2005). In contrast, open-coast cases like the 2018 Anak Krakatau and the 2002 Stromboli landslides and tsunami, are rapid subaerial or submarine mass movements that generated maximum near-field tsunami run-up heights of approximately 13.5 and ~11m from landslides

https://doi.org/10.5194/egusphere-2026-2543
Preprint. Discussion started: 22 June 2026

in the order of 10^7 m^3. Although the Pilar landslide involved a smaller volume than many of these events in Tab. 3, the observed maximum run-up of T1 (11.7 m) falls within the range of the open-coast volcanic cases.

Table 3. Comparison of selected landslide-generated tsunami events

Event Location	Trigger	Setting	Estimated Volume of Landslide (m^3)	Landslide Velocity (m/s) *modelled	Max wave Runup (m)	Key Controls	Reference
1958 Lituya Bay, USA	Earthquake-triggered rockslide	Confined fjord	~3× 10^7	110*	524	Extreme confinement, very steep impact slope, short source to impact distance	Miller (1960); Fritz et al. (2009); Weiss et al. (2009)
1963 Vajont Dam, Italy	Slope failure (reservoir-induced)	Artificial reservoir	~2–3 × 10^8	~16–30	~200–235	Basin confinement, very large slide, displacement wave	Semenza (2002) in Panizzo et al. (2005); Genevois and Tecca (2011)
2018 Anak Krakatau, Indonesia	Volcanic eruption-related flank collapse	Open coast	1.75–3.0 × 10^8	16.5*	13.5	Large sector collapse, mixed subaerial–submarine source, shallow shelf	Muhari et al., (2019); Grilli et al. (2019); Heidarzadeh et al. (2020); Hunt et al (2021)
2002 Stromboli, Italy	Dyke intrusion-triggered flank slides	Open coast	~1.1–2×10^7 ~0.4–1.35 ×10^7	30-60*	>11	Rapid mass entry on steep volcanic flank, partial coastal focusing	Tinti et al. (2006); Baldi (2008); Casalbore et al. (2020)
2017 Truong River, Vietnam	Rainfall-triggered slide	River	3.16 × 10^4	16	8.5	Rapid entry perpendicular to river channel	Duc et al. (2020)
2022 Pilar, Abuyog, Leyte, Philippines	Rainfall-triggered slide-debris flows	Semi-embayed coast	2.8–8.5 × 10^5	6–17+	11.7	Debris flow velocity, very short source to shore distance, partial focusing	This study
		River-dominated delta (new)	1.6–1.8 × 10^5	7–25	~8		
2022 Todos Los Santos, Chile	Rainfall-triggered landslide	Lake	1.05 × 10^4	5	0.8	Shallow and confined local bathymetry	Aranguiz et al. (2023)

Smaller (10^4 m^3) and also rainfall-triggered landslides have also generated waves in Todos Los Santos Lake (Aranguiz et al., 2023) and Truong River (Duc et al, 2020). While both also had confined configurations, these cases, along with Pilar example, highlight the need to study this type of hazard cascade. These suggest that landslide velocity and source proximity to the water

https://doi.org/10.5194/egusphere-2026-2543
Preprint. Discussion started: 22 June 2026

body can compensate for smaller volumes. In this sense, the Pilar event demonstrates that rainfall-triggered landslides in steep tropical volcanic terrains can generate tsunamis with runups comparable to those produced by eruption and intrusion-related volcanic landslides in open-coast settings, where wave generation is similarly controlled by landslide momentum rather than basin confinement.

Like the 2002 Stromboli event, the Pilar case also highlights the importance of multi-phase slope failure in landslide–tsunami systems. Sequential debris-flow events (DF1 and DF2) produced multiple tsunami wave trains (T1 and T2), with the first and largest event generating the highest runup. Although the second tsunami in Pilar was smaller, it remained hazardous and directly impacted rescue operations, underscoring the risks associated with temporally clustered failures in coastal environments. This behavior indicates that tsunami hazard in such settings should be treated as a sequence of closely spaced impacts rather than a single event.

Overall, the landslide–tsunami coupling observed in Pilar is consistent with established scaling relationships, wherein near-field tsunami amplitude increases with landslide momentum and decreases with increasing water depth and distance from the source. The Pilar event demonstrates that rainfall-triggered landslides, in addition to volcanic and tectonic processes, can generate destructive tsunamis in coastal settings, particularly in tropical island-arc environments where such events remain poorly documented. This underscores the need to incorporate landslide–tsunami cascade scenarios into hazard assessments in steep coastal terrains.

From a hazard assessment perspective, these findings indicate that approaches treating landslides and tsunamis as independent processes may not fully capture the risks posed by cascading events in coastal mountainous regions. Integrating landslide susceptibility with nearshore tsunami potential, particularly under conditions of prolonged rainfall, may therefore be necessary in similar environments.

6.4 Tsunami impacts and dominance in loss of life

Field observations and post-event surveys indicate that tsunami impacts in Barangay Pilar were characterized by strong, turbulent flow capable of transporting large debris and causing widespread structural damage. Run-up heights reaching up to ~11.7 MASL, combined with repeated wave arrivals, suggest highly energetic near-field conditions consistent with impulsive wave generation (Fritz et al., 2004; Heller and Hager, 2010).

Damage patterns provide insight into flow behavior. Coastal and nearshore structures exhibited evidence of both hydrodynamic loading and debris impact, including displacement of houses, stripping of vegetation, and lateral transport of materials. The presence of mixed sediments and organic debris in inundated areas indicates that tsunami flow was highly sediment-laden, reflecting continued input from the debris flow during wave generation. This is consistent with observations that later waves were more turbid and debris-rich than the initial wave.

https://doi.org/10.5194/egusphere-2026-2543
Preprint. Discussion started: 22 June 2026

Eyewitness accounts and video recordings indicate repeated submergence and strong turbulence, suggesting that flow velocities remained high during inundation and drawdown phases. Although direct measurements are not available, the observed damage and transport of large objects imply flow conditions capable of exerting substantial hydrodynamic forces. These observations are consistent with established tsunami impact models, in which flow depth, velocity, and debris load collectively control destructive potential.

Spatial variations in impact further reflect the influence of local coastal geometry. Greater damage and higher run-up were observed along the eastern sector of Barangay Pilar, consistent with the inferred directionality of debris-flow entry and partial wave focusing discussed in Section 6.3. In contrast, areas further from the primary impact zone experienced reduced inundation, indicating rapid attenuation of wave energy alongshore.

The sequence of multiple wave arrivals also contributed to cumulative damage. Initial waves caused primary inundation and structural failure, while subsequent waves remobilized debris and prolonged hazardous conditions. This multi-wave behavior is consistent with the multi-phase landslide sequence and highlights the importance of considering temporally clustered impacts in tsunami hazard assessment.

Overall, the observed impacts in Pilar reflect the combined effects of high flow velocity, significant debris loading, and localized wave focusing in a near-field setting. These characteristics underscore the destructive potential of landslide-generated tsunamis, even in the absence of large source volumes or strong basin confinement.

6.5 Implications for hazard assessment and disaster risk reduction

The Pilar disaster highlights fundamental limitations of hazard frameworks that treat landslides and tsunamis as independent phenomena. Although the community had preparations for a catastrophic landslide and for tsunamis, a landslide-induced tsunami, more so, two to three of them occurring within 2 hours, was not in their scenario. Previous studies emphasized that cascading and compound hazards can substantially amplify disaster impacts, particularly when response strategies optimized for one hazard inadvertently increase exposure to another (Gill and Malamud 2014; Day and Fearnley, 2015).

For the Philippines and similar archipelagic regions, hazard assessments should explicitly identify coastal slopes capable of generating tsunamis upon failure and integrate rainfall thresholds, high-resolution topography, and landslide–tsunami scenario modeling (Løvholt et al., 2020; Hungr et al., 2014). The permanent relocation of Barangay Pilar following the disaster underscores the limits of short-term and structural risk reduction measures in extremely high-risk coastal settings.

https://doi.org/10.5194/egusphere-2026-2543
Preprint. Discussion started: 22 June 2026

7 Conclusions

This study describes the first well-documented subaerial landslide-generated tsunami in the Philippines, triggered by prolonged and intense rainfall associated with the interaction of a low pressure area, Severe Tropical Storm Megi (Agaton), and Typhoon Malakas (Basyang) in April 2022. The Pilar, Abuyog disaster demonstrates how rainfall-driven slope failures in steep, tectonically fractured, volcaniclastic terrains can rapidly cascade into high-impact coastal hazards, even in the absence of strong seismic or volcanic triggers. This event provides a rare, data-rich example of a rainfall–landslide–tsunami cascade in a tropical island arc setting.

The integrated reconstruction using field observations, UAV-derived terrain models, satellite imagery, sedimentological analyses, eyewitness accounts, and video records reveals that the event involved at least two distinct debris flow phases occurring within a short time window. Progressive rainfall-induced pore-pressure buildup, long-term slope preconditioning, and fault-related structural weakening contributed to initial slope failure, which rapidly transformed into highly mobile debris flows. The first and larger debris flow entered the coastal zone with sufficient volume and momentum to generate a destructive near-field tsunami, producing runup heights of up to approximately 12 m above mean sea level. A second, more channelized debris flow generated a subsequent, lower-amplitude tsunami that nonetheless posed significant danger, including direct impacts on rescue operations.

Analysis of landslide–tsunami coupling indicates that tsunami generation in Pilar was governed primarily by high-momentum impact conditions, with debris-flow velocities of up to 25 m/s and very short source-to-shore distances limiting energy dissipation prior to coastal entry. These conditions resulted in strongly supercritical flow and impulsive wave generation, demonstrating that relatively moderate-volume landslides can produce significant near-field tsunamis when velocity and proximity are favorable (Fritz et al., 2004; Heller and Hager, 2010; Løvholt et al., 2015).

The Pilar case highlights the disproportionate role of landslide-generated tsunamis in controlling loss of life during rainfall-induced landslide disasters in coastal settings. While the landslide itself caused extensive burial and structural damage, tsunami inundation dominated mortality patterns due to extremely short warning times, high flow velocities, and the proximity of the landslide source to the shoreline. This observation is consistent with previous studies of near-field tsunami impacts, where rapid onset and limited evacuation time significantly increase fatality rates (e.g., Synolakis and Bernard, 2006; Fritz et al., 2009). Critically, evacuation guidance appropriate for landslide hazards—specifically movement toward the coast—unintentionally increased exposure to tsunami impacts, underscoring the challenges posed by compound and cascading hazards.

From a hazard assessment perspective, the results emphasize the need to move beyond single-hazard frameworks and explicitly incorporate landslide–tsunami coupling into landslide susceptibility mapping, rainfall-based early warning systems, and contingency planning. More broadly, the Pilar event demonstrates that rainfall-triggered slope failures in steep coastal

https://doi.org/10.5194/egusphere-2026-2543
Preprint. Discussion started: 22 June 2026

environments should be recognized as credible tsunami sources, particularly in humid tropical regions where prolonged rainfall can rapidly destabilize volcaniclastic terrains. In tropical island-arc regions such as the Philippines, where steep volcanic terrains commonly abut densely populated coastlines, systematic identification of coastal slopes capable of generating tsunamis upon failure is essential. High-resolution topographic data, structural mapping, and scenario-based modelling of sequential debris flows and tsunami generation should form part of future risk assessments.

The permanent relocation of Barangay Pilar following the disaster reflects the limits of short-term evacuation and structural mitigation measures in extremely high-risk coastal environments. As climate change is expected to intensify extreme rainfall events in the region (IPCC, 2021), rainfall-triggered landslide tsunamis are likely to represent an increasing and under-recognized threat. Integrating landslide susceptibility with nearshore tsunami potential, particularly under extreme rainfall scenarios, will be critical for improving risk reduction strategies in similar settings. The Pilar landslide tsunami thus provides a critical reference case for understanding the processes, impacts, and risk-reduction challenges associated with cascading landslide–tsunami hazards in tropical coastal settings.

In this context, the Pilar event indicates that rainfall-triggered landslides in steep tropical coastal environments can generate destructive tsunamis through rapid, high-mobility debris-flow impacts. This expands the range of recognized tsunami-generating processes beyond tectonic and volcanic sources and highlights the importance of considering cascading hazards in coastal settings. In regions characterized by steep slopes, high rainfall, and densely populated shorelines, approaches that integrate slope instability with nearshore wave generation may be necessary to fully capture hazard potential.

Code, data, or code and data availability

All drone images and processing code, waypoints and field photos from the UP Resilience Institute Team are accessible via the UP Resilience Institute online repository for Leyte Fieldwork 2022: https://drive.google.com/drive/folders/1gJTtA-B1RhsGn5ZHALrrt4PBXZID_9sD. Sampling sites and analysis are in the Abuyog Samples, Shapefiles and Models drive folder: https://drive.google.com/drive/folders/1gJTtA-B1RhsGn5ZHALrrt4PBXZID_9sD; before publication, downloading access to these Google Drive folders is limited to reviewers. After the review process and manuscript publication, all these files will be linked to the University of the Philippines Nationwide Operational Assessment of Hazards (UP NOAH) Open File Reports and the UP Resilience Institute Katatagan Database (currently under development).

Supplement link

Supplementary figures are accessible through this link: https://drive.google.com/drive/folders/1_MUhK4JUSlZqLWDZYKY7XyEMTEGVwOgg?usp=drive_link.

https://doi.org/10.5194/egusphere-2026-2543
Preprint. Discussion started: 22 June 2026

Author contributions

Likha G. Minimo[1,2] co-led and conducted the landslide investigation and interviews, guided the targeting of sites for the drone survey, transcribed, translated and coded the interview recordings, curated and analysed data from all teams, funded the sediment analysis, created 3D geologic models in Leapfrog, led and created the majority of the visualization, wrote parts of methodology and majority of results sections, conceptualized, led and facilitated the review and editing of the manuscript.

Janneli Lea A. Soria[3] co-led and conducted the tsunami investigation and interviews, analysed data from the tsunami survey team and landslide samples, created figures for visualization of tsunami heights and sediment analysis, conceptualized and wrote the draft sections on related literature, methodology, tsunami survey, and discussion, reviewed, and edited the manuscript.

Richard L. Ybanez[1] processed and analysed UAV/drone imagery, generated digital surface models and finalized geologic maps, and reviewed and edited the manuscript.

Audrei Anne B. Ybanez[1] facilitated the administration of the fieldwork preparations, led the writing of the introduction and background sections, and contributed to the overall critical review and editing of the manuscript.

Angelu B. Bermas[1] led the administration of the fieldwork and sample analysis, conducted the landslide investigation, drone survey, and interviews, wrote and created a visualization for the draft section on rainfall data, geology and lineament analysis.

Kayla Milcah M. Marasigan[1] facilitated the administration of the fieldwork, conducted the tsunami investigation and interviews, and wrote and created a visualization for the draft section on the study area and geological setting.

Adrian Gelo F. Tianchon[1] conducted the landslide investigation, drone survey, and interviews, and wrote and created a visualization for the draft section on cyclone data.

Jannine T. Vasquez[1] conducted the tsunami investigation and interviews and contributed to the draft section on the study area and geological setting.

Victor M. Romero II[4] led and conducted the drone survey, wrote and executed the code for drone data processing, and wrote part of the methodology draft.

Allan N. Amistoso[4] conducted the drone survey, wrote and executed the code for drone data processing.

Christer Kim O. Gerona[4†] assisted in the drone survey, transcribed and translated interviews before passing away in April 2023.

Genaro A. Cuaresma[5] assisted in the landslide and tsunami field investigation.

Alfredo Mahar Francisco A. Lagmay∗[1,6] led the conceptualization of the paper, co-led the field investigation and interviews, acquired funding for the fieldwork, wrote the original draft, and most of the discussion section, and led the review and editing of the manuscript.

Competing interests

Richard Ybanez is a PhD student of NHESS Executive Editor Dr. Bruce D. Malamud in the UP NIGS. Dr. Alfredo Mahar Francisco A. Lagmay is the main supervisor of Mr. Ybañez in the same research. No other competing interest is known to the authors.

https://doi.org/10.5194/egusphere-2026-2543
Preprint. Discussion started: 22 June 2026

Acknowledgements

The team expresses our gratitude to the Abuyog LGU, Leyte Provincial Government, Pilar, Bahay, and Malaguicay residents for the support we received during the fieldwork, their consent, data provision, and interview participation. Majority of the administration of the fieldwork and data processing were done in and through the UP Resilience Institute Knowledge Sharing Division and NOAH Hazards Assessment Team. We also thank the Central Visayan Institute Foundation (CVIF), UPD Science and Society Program, and UP Tacloban College for the participation of their faculty members in this research. We also acknowledge the sediment sample analysis by the UP NIGS Nannoworks Laboratory and Geotechnica Corp., and the transcription and translation of interviews by Kent Elizar Duan of UP Tacloban and UPRI Knowledge Sharing Interns Anna Joy Simon & John Aramil.

Financial support

Funding: Fieldwork in Leyte and sample analysis were funded by UP Resilience Institute Hazard Assessment Team, Dr. Lagmay, and Dr. Minimo.

References

Abuyog Municipal Disaster Risk Redcution and Management Office: Tropical Storm Agaton landslide situational report. Municipality of Abuyog, Leyte, 2022.

Allen, C.R.: Circum-Pacific faulting in the Philippines–Taiwan region, Journal of Geophysical Research, 67, 4795–4812, https://doi.org/10.1029/JZ067i012p04795, 1962.

Aránguiz, R., Caamaño, D., Espinoza, M., Gómez, M., Maldonado, F., Sepúlveda, V., Rogel, I., Oyarzun, J. C. and Duhart, P.: Analysis of the cascading rainfall–landslide–tsunami event of June 29th, 2022, Todos los Santos Lake, Chile. Landslides, 20(4), 801-811, https://doi.org/10.1007/s10346-022-02015-1, 2023.

Bahay Jeep ni Antet: This Entire Village was Buried Alive | Jeepney House Philippine Loop|, Leyte, Abuyog. Youtube, https://youtu.be/KXiC1bYSHIg?si=TUxHCNHJM3QJ10zS&t=1492, (last access 20 June 2026), 2024.

Baldi, P., Bosman, A., Chiocci, F.L., Marsella, M., Romagnoli, C., Sonnessa, A.:Integrated subaerial-submarine morphological evolution of the Sciara del Fuoco after the 2002 landslide. In: The Stromboli Volcano: An Integrated Study of the 2002–2003 Eruption. American Geophysical Union, Geophysical Monograph, Series, 171–182, 2008.

https://doi.org/10.5194/egusphere-2026-2543
Preprint. Discussion started: 22 June 2026

Blott, S.J., and Pye, K.: Gradistat: A Grain Size Distribution and Statistics Package for the Analysis of Unconsolidated Sediments. Earth Surface Processes and Landforms, 26, 1237-1248, http://dx.doi.org/10.1002/esp.261, 2001.

Bureau of Fire Protection Region 8: IN FRAME: Ongoing rescue operation at Brgy. Pilar, Abuyog, Leyte wherein another landslide occurred this afternoon at said area, https://www.facebook.com/100064847132048/videos/pcb.350358077135761/2119315464893710, April 12, 2022.

Casalbore, D., Romagnoli, C., Bosman, A., and Anzidei, M.: Submarine mass movements and their relationship with active volcanic structures at Stromboli volcano (Italy), *Earth-Science Reviews*, 204, 103161, 2020.

Casalbore, D., Passeri, F., Tommasi, P., Verrucci, L., Bosman, A., Romagnoli, C., Chiocci, F. L.: Small-scale slope instability on the submarine flanks of insular volcanoes: the case-study of the Sciara del Fuoco slope (Stromboli), International Journal of Earth Sciences, 109, 2643–2658, https://doi.org/10.1007/s00531-020-01853-5, 2020.

Day, S., and Fearnley, C.: A classification of mitigation strategies for natural hazards: implications for the understanding of interactions between mitigation strategies. Natural Hazards, 79(2), 1219-1238, DOI 10.1007/s11069-015-1899-z, 2015.

Delcamp, A., Roberti, G., and van Wyk de Vries, B. Water in volcanoes: evolution, storage and rapid release during landslides. Bulletin of Volcanology, 78, 87, https://doi.org/10.1007/s00445-016-1082-8, 2016.

Department of Science and Technology-Advanced Science and Technology Institute, and Philippine Space Agency: Landslide-Affected Areas: Brgy. Pilar, Abuyog Leyte: April 16, 2022, https://www.facebook.com/DATOSproject/photos/a.675209966147150/1659155907752546/, 2022

Dohmen, K., Blum, P., Braun, A., & Fernandez-Steeger, T. M.: Landslide-triggered tsunamis–a review. *Natural Hazards*, *121*(19), 22341-22373, https://link.springer.com/content/pdf/10.1007/s11069-025-07551-2.pdf, 2025.

Duc, D. M., Khang, D. Q., Duc, D. M., Ngoc, D. M., Quynh, D. T., Thuy, D. T., Giang, N. K. H, Tien P. V. and, Ha, N. H: Analysis and modeling of a landslide-induced tsunami-like wave across the Truong river in Quang Nam province, Vietnam. Landslides, 17(10), 2329-2341. https://doi.org/10.1007/s10346-020-01434-2, 2020.

Fritz, H. M., Hager, W. H., & Minor, H. E.: Near field characteristics of landslide-generated impulse waves. Journal of waterway, port, coastal, and ocean engineering, 130(6), 287-302, https://doi.org/10.1061/(ASCE)0733-950X(2004)130:6(287), 2004.

https://doi.org/10.5194/egusphere-2026-2543
Preprint. Discussion started: 22 June 2026

Fritz, H. M., Kongko, W., Moore, A., McAdoo, B., Goff, J., Harbitz, C., Uslu, B., Kalligeris, N., Suteja, D., Kalsum, K., Titov, V., Gusman, A., Latief, H., Santoso, E., Sujoko, S., Djulkarnaen, D., Sunendar, H., and Synolakis, C.: Extreme runup from the 17 July 2006 Java tsunami. Geophysical Research Letters, 34(12), doi:10.1029/2007GL029404, 2007.

Fritz, H. M., Mohammed, F., & Yoo, J.: Lituya Bay landslide impact generated mega-tsunami 50th anniversary. In Tsunami science four years after the 2004 Indian Ocean tsunami: Part II: Observation and data analysis, Basel, Birkhäuser Basel, 153-175, https://doi.org/10.1007/978-3-0346-0064-4_9, 2009.

General Bathymetric Charts of the Oceans: The GEBCO 08 115 0 130 25 Grid version 20091120, 2009.

Genevois, R. and Tecca, P. R.: The Vajont landslide: state of the art, *Rock Mechanics and Rock Engineering*, 44, 363–402, 2011.

Gervasio, F.C.: Geotectonic developments of the Philippines. Journal of the Geological Society of the Philippines 25:18–38, 1971.

Glademer: Exploring the hidden gem of abuyog leyte Philippines PH | Premium Province, Youtube, https://youtu.be/pImtEaDD_TQ?si=suLj-sKc9_hQQfhe&t=553, (last access 20 June 2026), 2025.

Global Administrative Areas: GADM database of Global Administrative Areas, version 2.0. Available online: https://gadm.org/, 2012

Google Earth: April 16, 2022 Satellite imagery of Leyte, Latitude: 10°37'20.00" N - 10°43'40.00" N, Longitude: 124°53'0.00"E - 125°6'45.00"E, 2022.

Google Earth: July 31, 2023 Satellite imagery of Philippine Archipelago and Philippine Sea, Latitude: 4° N - 27° N, Longitude: 106°E - 150°E, 2023.

Grilli, S.T., Tappin, D.R., Carey, S., Watt, S.F., Ward, S.N., Grilli, A.R., Engwell, S.L., Zhang, C., Kirby, J.T., Schambach, L. and Muin, M.: Modelling of the tsunami from the December 22, 2018 lateral collapse of Anak Krakatau volcano in the Sunda Straits, Indonesia. Scientific Reports, 9(1), 11946, https://doi.org/10.1038/s41598-019-48327-6, 2019

Harbitz, C. B., Løvholt, F., Bungum, H. (2014) Submarine landslide tsunamis: how extreme and how likely? Natural Hazards 72, 1341–1374, https://doi.org/10.1007/s11069-013-0681-3, 2014.

Heller, V., & Hager, W. H.: Impulse product parameter in landslide generated impulse waves. *Journal of waterway, port, coastal, and ocean engineering*, *136*(3), 145-155, 2010.

https://doi.org/10.5194/egusphere-2026-2543
Preprint. Discussion started: 22 June 2026

780 Heller, V. and Ruffini, G., 2023. A critical review about generic subaerial landslide-tsunami experiments and options for a needed step change. Earth-Science Reviews, 242, 104459, https://doi.org/10.1016/j.earscirev.2023.104459, 2023.

Heidarzadeh, M., Ishibe, T., Sandanbata, O., Muhari, A. and Wijanarto, A.B.: Numerical modeling of the subaerial landslide source of the 22 December 2018 Anak Krakatoa volcanic tsunami, Indonesia. Ocean Engineering, 195, 106733, 2020.

Highland, L.M. and Bobrowsky, P.: The landslide handbook-A guide to understanding landslides (No. 1325). US Geological
785 Survey, 2008.

Heidarzadeh, M., Muhari, A., and Wijanarto, A. B.: Insights on the source of the 22 December 2018 Sunda Strait tsunami, Indonesia based on spectral analyses and numerical modelling, Pure and Applied Geophysics, 177, 409–428, 2020.

Hunt, J.E., Tappin, D.R., Watt, S.F.L. et al.: Submarine landslide megablocks show half of Anak Krakatau island failed on December 22nd, 2018. Nat Commun 12, 2827, https://doi.org/10.1038/s41467-021-22610-5, 2021.

790 Intergovernmental Panel on Climate Change (IPCC). (2021). Climate change 2021: The physical science basis. Contribution of Working Group I to the Sixth Assessment Report of the Intergovernmental Panel on Climate Change. Cambridge University Press.

Iverson, R.M., Reid, M.E., and LaHusen, R.G.: Debris flow mobilization from landslides. Annual Review of Earth and Planetary Sciences, 25(1), 85-138, https://doi.org/10.1146/annurev.earth.25.1.85, 1997.

795 Iverson, R. M.: Regulation of landslide motion by dilatancy and pore pressure feedback, Journal of Geophysical Research, 110, F02015, doi:10.1029/2004JF000268, 2005.

Iverson, R.M.: Landslide triggering by rain infiltration. Water resources research, 36(7), pp.1897-1910, 2000.

Jakob, M., Hungr, O. and Jakob, D.M.: Debris flow hazards and related phenomena, 1st edition, Springer Berlin, Heidelberg, p.700., https://doi.org/10.1007/b138657, 2005.

800 Japan Aerospace Exploration Agency: JAXA Global Rainfall Watch (GSMaP). Earth Observation Research Center. https://sharaku.eorc.jaxa.jp/GSMaP/, 2022.

Katayama, N.: Old records of natural phenomena concerning the “Shimabara Catastrophe” (in Japanese with English abstract): science reports of the Shimabara Volcano Observatory. Technical report, Kyushu University, Faculty of Science, 1974.

https://doi.org/10.5194/egusphere-2026-2543
Preprint. Discussion started: 22 June 2026

Lagmay, A.M.F.A., Tejada, L.G., Pena, R.E., Aurelio, M., Davy, B., David, S., and Billedo, E.: New definition of Philippine plate boundaries, Journal of the Geological Society of the Philippines, 64, 17–30, 2009.

Lewis, D.W., and McConchie, D.: Analytical sedimentology, Springer Science & Business Media, 2012.

Leyte Provincial Disaster Risk Reduction and Management Office: Situational report on Tropical Storm Agaton. Provincial Government of Leyte, 2022.

Løvholt, F., Pedersen, G., Harbitz, C. B., Glimsdal, S., and Kim, J: On the characteristics of landslide tsunamis. Philosophical Transactions of the Royal Society, 373 (2053), 20140376, https://doi.org/10.1098/rsta.2014.0376, 28 October 2015.

Løvholt, F., Glimsdal, S. and Harbitz, C.B.: On the landslide tsunami uncertainty and hazard, Landslides, 17(10), 2301-2315, https://doi.org/10.1007/s10346-020-01429-z, 2020.

Manegdeg, N.: How we conducted tsunami drills in all tsunami-prone schools in the Eastern Visayas, UNDP in Asia and the Pacific, Medium.com, https://medium.com/undp-in-asia-and-the-pacific/how-we-conducted-tsunami-drills-in-all-tsunami-prone-schools-in-the-eastern-visayas-95e5ca38644e, 2018.

Miller, D. J.: Giant Waves in Lituya Bay, Alaska, U.S. Geological Survey Professional Paper 354 C, 51 pp., 1960.

Mines and Geosciences Bureau: Geology of the Philippines, 2nd ed, Mines and Geosciences Bureau, Department of Environment and Natural Resources, Quezon City, 2010.

Mines and Geosciences Bureau Region VIII: Post-disaster geohazard assessment report on landslide-affected areas due to Tropical Storm Agaton, Abuyog, Leyte, 2022.

Muhari, A., Heidarzadeh, M., Susmoro, H., Nugroho, H., Kriswati, E., Supartoyo, Wijinarto, A.B., Imamura, F., and Arikawa, T.: The December 2018 Anak Krakatau Volcano Tsunami as Inferred from Post-Tsunami Field Surveys and Spectral Analysis. *Pure Appl. Geophys.* **176**, 5219–5233 (2019). https://doi.org/10.1007/s00024-019-02358-2, 2019.

National Mapping and Resource Information Authority: Topographic Map of Abuyog Quadrangle. http://www.namria.gov.ph/download.php, 1956

National Mapping and Resource Information Authority: The Philippine IfSAR project. Internal report jointly by NAMRIA, Intermap Technologies Inc. (Denver CO) and Certeza Infosys Corp. Technical report, NAMRIA Main Office, Taguig City, Philippines, 2013.

https://doi.org/10.5194/egusphere-2026-2543
Preprint. Discussion started: 22 June 2026

National Disaster Risk Reduction and Management Council: Situational Report No. 8 for TC AGATON (2022), April 16, 2022 08:00 am, https://reliefweb.int/report/philippines/ndrrmc-situational-report-no-8-tropical-storm-agaton-2022-april-16-2022-0800-am, 2022.

Okal, E.A. and Synolakis, C.E.: Source discriminants for near-field tsunamis. Geophysical Journal International, 158(3), 899-912, https://doi.org/10.1111/j.1365-246X.2004.02347.x, 2004.

Panizzo, A., De Girolamo, P., Di Risio, M., Maistri, A., & Petaccia, A.: Great landslide events in Italian artificial reservoirs, Natural Hazards and Earth System Sciences, 5(5), 733-740, https://nhess.copernicus.org/articles/5/733/2005/nhess-5-733-2005.pdf, 2005

Paris, R., Switzer, A. D., Belousova, M., Belousov, A., Ontowirjo, B., Whelley, P. L., & Ulvrova, M.: Volcanic tsunami: a review of source mechanisms, past events and hazards in Southeast Asia (Indonesia, Philippines, Papua New Guinea). *Natural Hazards*, *70*(1), 447-470, 2014.

Philippine Atmospheric, Geophysical and Astronomical Services Administration: Tropical Cyclone Preliminary Summary Tropical Storm Agaton (2022 Megi), https://pubfiles.pagasa.dost.gov.ph/pagasaweb/files/tamss/weather/tcprelimsummary/AGATON.pdf, 2022.

Philippine Institute of Volcanology and Seismology: Active volcanoes. http://www.phivolcs.dost.gov.ph/index.php?option=com_content&view=article&id=57:acti ve-volcanoes&catid=55&Itemid=114, 2008a.

Philippine Institute of Volcanology and Seismology: Active Faults and Trenches, PHIVOLCS website, 2008b.

Philippine Institute of Volcanology and Seismology: Earthquake Catalog, PHIVOLCS website, https://earthquake.phivolcs.dost.gov.ph/EQLatest-Monthly/2022/2022_April.html, 2022.

Qu, H., Dong, W., Wang, D., Zhang, Z. and Zhang, W.: Slope response characteristics under the coupled action of rainfall and earthquake: a case study with numerical modelling. Geotechnical and Geological Engineering, 41(4), 2501-2515,

Reid, J., and Mooney, W.:Tsunami occurrence 1900–2020: A global review, with Examples from Indonesia, Pure and Applied Geophysics, 2023.

Sajona, F.G., Bellon, H., Maury, R.C., Pubellier, M., Quebral, R.D., Cotten, J., Bayon, F.E., Pagado, E. and Pamatian, P.: Tertiary and quaternary magmatism in Mindanao and Leyte (Philippines): geochronology, geochemistry and tectonic setting. Journal of Asian Earth Sciences, 15(2-3), 121-153, https://doi.org/10.1016/S0743-9547(97)00002-0, 1997.

https://doi.org/10.5194/egusphere-2026-2543
Preprint. Discussion started: 22 June 2026

Sassa, K., Fukuoka, H., Wang, F., Wang, G.: Landslides Induced by a Combined Effect of Earthquake and Rainfall. In: Sassa, K., Fukuoka, H., Wang, F., Wang, G. (eds) Progress in Landslide Science. Springer, Berlin, Heidelberg. https://doi.org/10.1007/978-3-540-70965-7_14, 2007.

Seequent: Leapfrog Geo 2023.2 3D geological modelling software - Seequent, https://www.seequent.com/products-solutions/leapfrog-geo/, 2023.

Semenza, E.: La storia del Vajont, raccontata dal geologo che ha scoperto la frana., Tecomproject, Ferrara, 2002.

Synolakis, C., Okal, E. and Bernard, E.: The megatsunami of December 26, 2004. Bridge-Washington-National Academy of Engineering, 35(2), 27-35, 2005.

Synolakis, C.E. and Bernard, E.N.: Tsunami science before and beyond Boxing Day 2004. Philosophical Transactions of the Royal Society A: Mathematical, Physical and Engineering Sciences, 364(1845), 2231-2265, https://doi.org/10.1098/rsta.2006.1824, 2006.

Tan, H. and Chen, S.: A hybrid DEM-SPH model for deformable landslide and its generated surge waves. Advances in water resources, 108, 256-276, https://doi.org/10.1016/j.advwatres.2017.07.023, 2017.

Tappin, D.R.: Mass Transport Events and Their Tsunami Hazard. In: Mosher, D.C., et al. Submarine Mass Movements and Their Consequences. Advances in Natural and Technological Hazards Research, vol 28. Springer, Dordrecht. https://doi.org/10.1007/978-90-481-3071-9_54, 2010.

Thomas, D. R.: A general inductive approach for analysing qualitative evaluation data. American Journal of Evaluation, 27(2), 237-246, https://doi.org/10.1177/1098214005283748, 2006.

Tinti, S., Pagnoni, G. & Zaniboni, F.: The landslides and tsunamis of the 30th of December 2002 in Stromboli analysed through numerical simulations. Bulletin of Volcanology, 68, 462–479 (2006). https://doi.org/10.1007/s00445-005-0022-9, 2006.

Tsutsumi, H., and Perez, J.S.: Large-scale active fault map of the Philippine fault based on aerial photograph interpretation, Active fault research, 2013(39), pp.29-37, 2013.

United Nations Development Program Philippines: RAPID Program Earthquake and Tsunami Drill, https://www.facebook.com/watch/?v=599772374229380, 2020.

https://doi.org/10.5194/egusphere-2026-2543
Preprint. Discussion started: 22 June 2026

United Nations Educational, Scientific and Cultural Organization: International Tsunami Survey Team (ITST) post-tsunami survey field guide, 2nd Edition, IOC Manuals and Guides, 37, 114 pp, https://unesdoc.unesco.org/ark:/48223/pf0000229456, 2014

University of the Philippines Nationwide Operational Assessment of Hazards: Flood, Landslide and Storm Surge Hazard maps, https://noah.up.edu.ph/noah-studio, 2024.

United States Geological Survey: Shuttle Radar Topography Mission, 1 Arc Second scene SRTM_60_09, SRTM_60_10, SRTM_60_11, SRTM_61_09, SRTM_61_10, SRTM_61_11, SRTM_62_10 and SRTM_62_11, Unfilled Unfinished 2.0, Global Land Cover Facility, University of Maryland, College Park, Maryland, www.landcover.org, 2004.

Weiss, R., Fritz, H. M., and Wünnemann, K.: Hybrid modeling of the mega-tsunami runup in Lituya Bay after half a century, *Geophysical Research Letters*, 36, L09602, 2009.

Widiyanto, W., Hsiao, S.C., Chen, W.B., Santoso, P.B., Imananta, R.T. and Lian, W.C.: Runup, inundation, and sediment characteristics of the 22 December 2018 Sunda Strait tsunami, Indonesia, Natural Hazards and Earth System Sciences, 20(4), 933-946, https://doi.org/10.5194/nhess-20-933-2020, 2020

Ybañez, R.L., Ybañez, A.A.B., Lagmay, A.M.F.A. and Aurelio, M.A.: Imaging ground surface deformations in post-disaster settings via small UAVs, Geoscience Letters, 8(1), 23, https://doi.org/10.1186/s40562-021-00194-8, 2021.